# Analytic post-Newtonian expansion of the energy and angular momentum radiated to infinity by eccentric-orbit nonspinning extreme-mass-ratio inspirals to the 19th order

Christopher Munna

*Department of Physics and Astronomy, University of North Carolina, Chapel Hill, North Carolina 27599, USA*

(Received 30 August 2020; accepted 16 October 2020; published 1 December 2020)

We develop new high-order results for the post-Newtonian (PN) expansions of the energy and angular momentum fluxes at infinity for eccentric-orbit extreme-mass-ratio inspirals on a Schwarzschild background. The series are derived through direct expansion of the Mano-Suzuki-Takasugi solutions within the Regge-Wheeler-Zerilli formalism for first-order black hole perturbation theory (BHPT). By utilizing factorization and a few computational simplifications, we are able to compute the fluxes to 19PN, with each PN term calculated as a power series in (Darwin) eccentricity to $e^{10}$. This compares favorably with the numeric fitting approach used in previous work. We also compute PN terms to $e^{20}$ through 10PN. Then, we analyze the convergence properties of the composite energy flux expansion by checking against numeric data for several orbits, both for the full flux and also for the individual 220 mode, with various resummation schemes tried for each. The match between the high-order series and numerical calculations is generally strong, maintaining relative error better than $10^{-5}$ except when $p$ (the semilatus rectum) is small and $e$ is large. However, the full-flux expansion demonstrates superior fidelity (particularly at high $e$), as it is able to incorporate additional information from PN theory. For the orbit $(p = 10, e = 1/2)$, the full flux achieves a best fractional error near $10^{-5}$, while the 220 mode exhibits error worse than 1%. The full series can be accessed electronically on the black hole perturbation toolkit and are also given as Supplemental Material. Finally, we describe a procedure for transforming these expansions to the harmonic gauge of PN theory by analyzing Schwarzschild geodesic motion in harmonic coordinates. This will facilitate future comparisons between BHPT and PN theory.

DOI: 10.1103/PhysRevD.102.124001

## I. INTRODUCTION

With the launch of the LISA mission rapidly approaching, advancements in our understanding of generic extreme-mass-ratio inspirals (EMRIs), a major source of gravitational waves in LISA's frequency band, are of paramount importance [1–4]. Theoretical models of these systems permit the creation of waveform templates, which can then be used to isolate gravitational-wave signals from LISA's data stream. If sufficiently accurate, these templates can also be used to estimate various characteristics of the bodies.

To aid this effort, the past few decades have seen significant research in the field of black hole perturbation theory (BHPT), in which the Einstein field equations are expanded under the assumption that one of the two masses is much larger than the other, or $\mu/M \ll 1$. In this approximation the zeroth-order system is given by the spacetime of the large central black hole (Schwarzschild or Kerr), with the smaller body following a geodesic on that background. The geodesic motion of the smaller body sources the first-order perturbation, which then interacts with the body itself, causing a self-force or radiation reaction, driving the two bodies together. See [5] for a review. By design this scheme is naturally suited to the description of EMRIs; however, the expansion process is quite complex. The first-order perturbation is effectively understood on both Schwarzschild [6–10] and Kerr [11–14], but neither is yet implemented computationally in a manner sufficient for LISA. Worse, the second-order solution is not yet known theoretically, though significant progress is being made [15–19]. Thus, much work remains before LISA data analysis can begin.

There is another approximation scheme that applies for binary systems with slowly moving (or equivalently, widely separated) bodies. This is the classic post-Newtonian (PN) expansion, which utilizes the small parameter $v/c \ll 1$ [20]. The PN approximation is accurate early in the lifetime of any inspiral but generally breaks down before the point of merger. Thus, this expansion method must be supplemented with additional information in order to capture the inspiral's full behavior. For the comparable-mass binaries observed by LIGO, the late-stage orbit is typically described using full numerical relativity (NR) simulations. Information from PN and NR (as well as BHPT) can be joined using a compact interpolation scheme known as the

 

effective-one-body (EOB) formalism [21–23]. The combination of the three (PN, NR, EOB) has led to a large library of waveform templates for LIGO, which have allowed for its unprecedented success in detecting and characterizing mergers (see, e.g., [24–29]). PN waveforms in particular were essential to the detection of the first binary neutron star merger [30], which heralded in a new era of multimessenger astronomy [31,32].

Once the mass ratio deviates from unity, models from BHPT become necessary for the construction of accurate waveform templates. This fact has already been validated through LIGO: Detections of $1/3.6$ mass ratio and $1/8.8$ mass ratio binaries [33,34] utilized EOB waveforms partially calibrated using BHPT [35–37]. For the EMRIs that will be observable by LISA, BHPT will almost surely serve as the central analytic framework in the construction of waveform templates. However, due to the theoretical and computational complexity of BHPT methods, some combination with the other approximation schemes may be required to achieve rapid, accurate simulations across the possible parameter space. To that end, there has recently been a surge in work at the intersection of BHPT and PN theory, with frequent application to EOB models [38–76]. As evidenced in those papers, combining the methodologies in this manner often yields progress in the separate theories that would be more difficult to derive otherwise.

The present work advances this effort by combining BHPT with PN theory to determine high-order PN series for the (orbit-averaged) energy and angular momentum radiated out to infinity by eccentric, nonspinning EMRIs. The expansions are pursued via the formalism of Mano, Suzuki, Takasugi (MST), which solves the Regge-Wheeler-Zerilli (RWZ) equations of first-order BHPT using infinite summations of analytic functions [6–8,77]. In particular, the MST solutions to the homogeneous RW equation contain small PN parameters with which expansions can be made rapidly using algebraic computing software such as *Mathematica* [50,54,78–81]. These series can then be joined with PN expansion of the source motion to compute analytic series for the normalization constants and fluxes. The resulting flux representations can be rapidly evaluated to produce numeric values along and across orbits. Related methods have already been successfully applied to extract high-order series for various orbital quantities in both the conservative and the dissipative sectors, on both Schwarzschild and Kerr backgrounds [43,44,49,51,54–58,61–70,74–76,82].

The fluxes serve as the largest contribution to the inspiral's orbital phase and therefore require high accuracy in the construction of waveforms [83,84], suggesting the utility of high-order expansions. In 2012 Fujita applied similar techniques to derive the circular-orbit limit of the EMRI energy flux to 22PN [44]. In the eccentric case each PN term must also be expanded as a Taylor series in Darwin eccentricity $e$ to complete the source integration, compounding the complexity by an order of magnitude. Nevertheless, because LISA is expected to be sensitive to binaries with moderate or high eccentricity (unlike LIGO, which primarily observes circular-orbit binaries), expansions which reach high orders in both $v/c$ and $e$ may be needed [2,85,86].

To that end, four other papers have also made recent progress on the eccentric EMRI flux expansions, though with different techniques [53,72,73,87]. Specifically, the two [53,87] utilized thousands of numeric flux calculations to perform numeric fits to the forms of the two PN expansions. These numeric fits were then partially converted to analytic form using an integer relation algorithm [88], resulting in series to 9PN and varying orders in eccentricity (frequently, $e^{30}$). The other two [72,73] combined separate discoveries from BHPT and PN theory to derive certain logarithmic contributions to the fluxes to arbitrary order in eccentricity.

The analytic expansion procedure of the present work confers several advantages over the fitting methods of [53,87], allowing us to extend those results to much higher PN order. In total, we compute each of the two fluxes to 10PN through $e^{20}$ and to 19PN through $e^{10}$, with the latter PN order nearing the state of the art for circular orbits [44]. As all PN series, these flux representations produce numeric values that are accurate early in the EMRI's lifetime; however, it has also more recently been found that sufficiently high-order expansions have the potential to match numerical calculations near the point of merger. Indeed, the authors of [44] found that the 22PN expansion of the circular-orbit fluxes was sufficient to track the inspiral's evolution all the way to the separatrix. Other works have demonstrated apparent convergence for certain conservative PN series everywhere outside the light ring of the system (with known singularities at the light ring) [48,56,89]. We therefore use the present results to assess whether analogous convergence properties hold for eccentric orbits, both for an individual mode as well as for the full flux. We evaluate different orbits and vary the PN order, and we also try a few resummation schemes such as those mentioned in [90] to compare fidelity.

We find that for the 220 mode flux, the expansion for $p = 10$ can be made to maintain relative error better than $10^{-6}$ for $e \lesssim 1/4$ by factoring out the separatrix $p - 6 - 2e$. However, at larger $e$ the series breaks down, barely reaching an error of 1% at $e = 1/2$ in the best case (though typically far worse). Wider orbits exhibit better fidelity. The full-flux expansion proves superior to the factorized mode flux, due to the fact that the former can incorporate derivations from PN theory and also utilize eccentricity singular factors. As a result, an error of roughly $10^{-5}$ can be achieved in the full flux at $(p = 10, e = 1/2)$. Because of the large size of the expressions, it will not be useful to supply them here; however, the full series are posted on the black hole perturbation toolkit in *Mathematica* format [91]. We have also provided them as Supplemental Material for

easy retrieval [92]. This effort serves as a necessary intermediate step on the path to fully generic expansions on a Kerr background.

It is of note that BHPT-PN series reproduce the small-mass-ratio limit of the full PN theory [20], but in terms of parameters suited to BHPT coordinate systems—such as the Darwin eccentricity $e$, semilatus rectum $p$, and relativistic anomaly $\chi$ in Schwarzschild coordinates. Direct comparisons to derivations within the full PN framework require transforming back to the more standard PN representation involving quasi-Keplerian (QK) parameters such as the time eccentricity $e_t$ or true anomaly $V$ in (modified) harmonic or Arnowitt-Deser-Misner (ADM) coordinates. This was generally said to be possible only to the highest known order of the full PN equations of motion. The equations of motion have been recently found to 4PN [93], though the quasi-Keplerian parameters have only been explicitly derived to 3PN [94–96]. This allows for the confirmation of mutual agreement between the two theories in low-order cases.

However, the litany of high-order BHPT-PN expansions, as well as of newer techniques permitting the extraction of PN terms in nonsequential order (often by combining BHPT and PN theory [41,42,53,75,75,97,98]), has made it desirable to be able to convert to and from QK harmonic parameters to higher order. This can be done by analyzing the harmonic-coordinate solution of the Schwarzschild metric. This solution will serve as the small-mass-ratio limit of full PN harmonic coordinates. We will show that the simple relationship between Schwarzschild harmonic coordinates and basic Schwarzschild coordinates can be used to form a QK representation of Schwarzschild geodesic motion to arbitrary order. This representation will give definition to the QK parameters to arbitrary PN order at lowest order in the mass ratio, allowing them to be connected to the BHPT expansion parameters to arbitrary order as well.

The structure of this paper is as follows. In Sec. II, we broadly review the RWZ formalism for generic bound orbits on a Schwarzschild background and discuss the significance of high-order flux series. Then, in Sec. III, we describe the analytic expansion of the MST homogeneous solutions, following the methods of [50,78,79]. In Sec. IV we proceed to the inhomogeneous problem, applying the techniques of [54,56]. Section V describes the flux results, which are then compared to numerical calculations to test the accuracy and convergence of the series. Section VI then describes the process by which these and other BHPT-PN expansions can be converted to a QK representation with harmonic-gauge parameters. We finish in Sec. VII with conclusions and outlook.

Unless otherwise noted, we set $c = G = 1$ and use metric signature $(-+++)$ and sign conventions of Misner, Thorne, and Wheeler [99]. Our notation for the RWZ formalism follows that found in [53,54,87], which in part derives from notational changes for tensor spherical harmonics and perturbation amplitudes made by Martel and Poisson [8]. For the MST formalism, we largely make use of the discussion and notation found in the review by Sasaki and Tagoshi [100].

## II. REVIEW OF THE RWZ FORMALISM AND FIRST-ORDER FLUXES

### A. The RWZ master equations

We begin by outlining the RWZ formalism used to compute the fluxes within first-order BHPT for a point mass $\mu$ in eccentric orbit around a Schwarzschild black hole of mass $M$ in the equatorial plane. We use Schwarzschild coordinates $x^\mu = (t, r, \theta, \varphi)$ with the line element

$$ds^2 = -f dt^2 + f^{-1} dr^2 + r^2(d\theta^2 + \sin^2\theta d\varphi^2) \tag{2.1}$$

for $f = (1 - 2M/r)$. The Schwarzschild metric is thus the zeroth-order piece of the full metric $g_{\mu\nu}$. To obtain the first-order portion, the RWZ approach decomposes the linearized field equations in RW gauge over tensor spherical harmonics with indices $lm$. The angular components decouple, resulting in two sets of partial differential equations (PDEs) for the $t$- and $r$-dependent spherical harmonic amplitudes, one for odd parity and the other for even parity. It is found that each set can be encoded to a single (mode-dependent) PDE for a corresponding master function. The first-order metric perturbations can then be recovered from these master functions. The reader should refer to [8,10] for a complete description.

The odd-parity PDE, known as the time domain (TD) RW equation, is given by

$$\left[-\frac{\partial^2}{\partial t^2} + f\frac{\partial}{\partial r} f \frac{\partial}{\partial r} + f\left(\frac{l(l+1)}{r^2} - \frac{6M}{r^3}\right)\right]\Psi^o_{lm} = S^o_{lm}, \tag{2.2}$$

where $\Psi^o_{lm}$ is the odd-parity master function. The source term results from the tensor spherical harmonic decomposition of the smaller body's (point particle) stress energy tensor. It can be written as

$$S^o_{lm}(t) = G^o_{lm}(t)\delta[r - r_p(t)] + F^o_{lm}(t)\delta'[r - r_p(t)], \tag{2.3}$$

for functions $G^o_{lm}(t)$ and $F^o_{lm}(t)$ that will be given explicitly in Sec. II C below.

Similarly, the even-parity Zerilli equation is given by

$$\left\{-\frac{\partial^2}{\partial t^2} + f\frac{\partial}{\partial r} f \frac{\partial}{\partial r} + \frac{f}{\Lambda^2}\left[\kappa^2\left(\frac{\kappa+2}{r^2} + \frac{6M}{r^3}\right) + \frac{36M^2}{r^4}\left(\kappa + \frac{2M}{r}\right)\right]\right\}\Psi^e_{lm} = S^e_{lm}. \tag{2.4}$$

where $\kappa = (l-1)(l+2)$, $\Lambda = \kappa + 6M/r$, and

$$S^e_{lm}(t) = G^e_{lm}(t)\delta[r - r_p(t)] + F^e_{lm}(t)\delta'[r - r_p(t)]. \quad (2.5)$$

We now exploit the biperiodicity of the source motion and make a transformation to the frequency domain (FD). In this way the odd-parity equation becomes

$$\left[f\frac{\partial}{\partial r}f\frac{\partial}{\partial r} + \omega^2 + f\left(\frac{l(l+1)}{r^2} - \frac{6M}{r^3}\right)\right]X_{lmn}(r) = Z_{lmn}(r), \quad (2.6)$$

where $\omega = \omega_{mn} = m\Omega_\varphi + n\Omega_r$ and

$$X_{lmn}(r) = \frac{1}{T_r}\int_0^{2\pi}\Psi^o_{lm}e^{i\omega t}dt,$$
$$Z_{lmn}(r) = \frac{1}{T_r}\int_0^{2\pi}S^o_{lm}e^{i\omega t}dt. \quad (2.7)$$

For simplicity $X_{lmn}(r)$ and $Z_{lmn}(r)$ are written without a superscript denoting odd parity, as we shall work almost exclusively in the odd-parity sector. The TD solutions are reconstructed in the usual way:

$$\Psi^o_{lm} = \sum_{n=-\infty}^{\infty}X_{lmn}(r)e^{-i\omega t},$$
$$S^o_{lm} = \sum_{n=-\infty}^{\infty}Z_{lmn}(r)e^{-i\omega t}. \quad (2.8)$$

The homogeneous solutions to (2.6) can be derived analytically using the MST method [77]. This leads to the pair of functions $X^+_{lmn} = X^{\rm up}_{lmn}$, with proper behavior for $r > r_p$, and $X^-_{lmn} = X^{\rm in}_{lmn}$, with proper behavior for $2M < r < r_p$. The subscript $p$ represents the location of the smaller body. Explicit representations for $X^\pm_{lmn}$ will be given in Sec. III. The corresponding even-parity homogeneous solutions can be found directly from $X^+_{lmn}$ and $X^-_{lmn}$ using the Detweiler-Chandrasekar transformation [101–104].

### B. Particular solution to the Regge-Wheeler equation

A suitable set of particular solutions for this problem can be found using the method of extended homogeneous solutions (EHS) [9,105]. Explicitly, the result is

$$X_{lmn} = C^+_{lmn}X^+_{lmn}(r)\Theta[r - r_p(t)] + C^-_{lmn}X^-_{lmn}(r)\Theta[r_p(t) - r], \quad (2.9)$$

where $\Theta$ is the Heaviside function and $C^\pm_{lmn}$ are constants. Even though (2.9) is not a valid solution to (2.6), the time-domain solution found by taking

$$\Psi^o_{lm} = \sum_{n=-\infty}^{\infty}X_{lmn}e^{-i\omega t} \quad (2.10)$$

is in fact a valid solution to its time-domain counterpart, as can be shown by direct evaluation [9]. The proper normalization constants are given by

$$C^\pm_{lmn} = \frac{1}{W_{lmn}T_r}\int_0^{2\pi}\left[\frac{1}{f_p}G^o_{lm}(t)X^\mp_{lmn} + \left(\frac{2M}{r_p^2 f_p^2}X^\mp_{lmn} - \frac{1}{f_p}\frac{dX^\mp_{lmn}}{dr}\right)F^o_{lm}(t)\right]e^{i\omega t}dt, \quad (2.11)$$

where $T_r$ is the period of radial libration and $W_{lmn}$ is the Wronskian,

$$W_{lmn} = f\frac{dX^+_{lmn}}{dr}X^-_{lmn} - f\frac{dX^-_{lmn}}{dr}X^+_{lmn}. \quad (2.12)$$

Note that the corresponding even-parity expression is identical, but with the even-parity source terms $G^e_{lm}$ and $F^e_{lm}$ and homogeneous functions $X^{\mp,e}_{lmn}$. Interestingly, it can be shown through direct evaluation that the Wronskian $W_{lmn}$ is parity independent. Note also that the various functions are evaluated at the location of the smaller body, meaning that it is necessary to possess compact expressions for the zeroth-order motion of body. This is simply the geodesic motion of a test mass on a Schwarzschild background.

### C. Bound orbits on a Schwarzschild background and the corresponding source terms

At zeroth order the motion is geodesic in the static background. The geodesic equations can be integrated to yield the four-velocity as

$$u^\alpha = \left(\frac{\mathcal{E}}{f_p}, u^r, 0, \frac{\mathcal{L}}{r_p^2}\right) \quad (2.13)$$

for energy $\mathcal{E}$ and angular momentum $\mathcal{L}$. The radial motion is found using the constraint on the four-velocity $u^\alpha u_\alpha = -1$, or

$$(u^r)^2 = \mathcal{E}^2 - f_p\left(1 + \frac{\mathcal{L}^2}{r_p^2}\right). \quad (2.14)$$

Bound orbits have $\mathcal{E} < 1$ and $\mathcal{L} > 2\sqrt{3}M$.

In Sec. IV the motion will be reparametrized using geometric features of the orbit to simplify the process of PN expansion. For now, the four-velocity (2.13) can be used to derive compact forms for the source terms. The process is straightforward though cumbersome, involving combinations of components of the stress energy tensor integrated over tensor spherical harmonics. The odd-parity source terms are found to be

$$F_o^{lm}(t) = \frac{32\pi\mu\mathcal{L}f_p^3(r_p^2+\mathcal{L}^2)}{(l-1)l(l+1)(l+2)\mathcal{E}^2 r_p^3} X_\varphi^{*lm},$$
$$G_o^{lm}(t) = \frac{32\pi\mu\mathcal{L}f_p}{(l-1)l(l+1)(l+2)\mathcal{E}^2 r_p^5}[\mathcal{L}\mathcal{E}r_p^2\dot{r}_p(-im) - f_p(5Mr_p^2+7M\mathcal{L}^2+(2\mathcal{E}^2-1)r_p^3-2\mathcal{L}^2 r_p)]X_\varphi^{*lm}. \quad (2.15)$$

Note that these expressions were published in [54]. The even-parity terms follow as

$$F_e^{lm}(t) = \frac{32\pi\mu f_p^3(r_p^2+\mathcal{L}^2)}{l(l+1)(r_p(l-1)(l+2)+6M)\mathcal{E}r_p} Y_{lm}^*,$$
$$\begin{aligned} G_e^{lm}(t) = {} & \frac{16\pi\mu f_p}{(l-1)l(l+1)(l+2)r_p^3((l-1)(l+2)r_p+6M)^2\mathcal{E}}[2f_p^2(l-1)(2+l)\mathcal{L}^2 r_p(6M+(l-1)(2+l)r_p) \\ & - f_p\mathcal{L}(6M+(l-1)(2+l)r_p)(\mathcal{L}(l+l^2-2m^2)(6M+(l-1)(2+l)r_p)+4i(l-1)(2+l)mr_p^2u^r) \\ & + (l-1)(2+l)r_p^2(\mathcal{E}^2(-60M^2-12(l-1)(2+l)Mr_p-(l-1)l(1+l)(2+l)r_p^2) \\ & + (12M^2+12l(1+l)Mr_p+(l-1)l(1+l)(2+l)r_p^2)(u^r)^2)]Y_{lm}^*. \end{aligned} \quad (2.16)$$

The definitions for the scalar spherical harmonic $Y_{lm}$ and vector spherical harmonic $X_\varphi^{lm}$ are given in [8]. Both are evaluated at the location of the smaller body.

### D. The energy and angular momentum radiated to infinity

The RWZ method leads to elegant expressions for the energy and angular momentum radiated out to infinity. These are described in [8] by analyzing the $r \to \infty$ limit of the metric perturbations. Explicitly, they are given by

$$\left\langle \frac{dE}{dt} \right\rangle^\infty = \frac{1}{64\pi}\sum_{lm}(l+2)(l+1)(l)(l-1)\langle|\dot{\Psi}_{lm}^e(t,r=\infty)|^2+|\dot{\Psi}_{lm}^o(t,r=\infty)|^2\rangle, \quad (2.17)$$

$$\left\langle \frac{dL}{dt} \right\rangle^\infty = \frac{1}{64\pi}\sum_{lm}(l+2)(l+1)(l)(l-1)(-im)\langle\Psi_{lm}^{*e}\dot{\Psi}_{lm}^e+\Psi_{lm}^{*o}\dot{\Psi}_{lm}^o\rangle. \quad (2.18)$$

The horizon fluxes are similar, except with evaluation at $r = 2M$.

These can be simplified further by rewriting the $\Psi$ functions in terms of their EHS Fourier sums. These will involve factors such as $C_{lmn}^+ X_{lmn}^+$ evaluated in the appropriate limits. However, it is easier to instead work with normalized homogeneous functions $\hat{X}_{lmn}^+$ which are constructed to approach unity at infinity. With these normalized functions, the flux summations simply become

$$\left\langle \frac{dE}{dt} \right\rangle^\infty = \frac{1}{64\pi}\sum_{lmn}(l+2)(l+1)(l)(l-1)\omega^2|C_{lmn}^+|^2, \quad (2.19)$$

$$\left\langle \frac{dL}{dt} \right\rangle^\infty = \frac{1}{64\pi}\sum_{lmn}(l+2)(l+1)(l)(l-1)m\omega|C_{lmn}^+|^2, \quad (2.20)$$

where the $C_{lmn}^+$ are now constructed by integrating $\hat{X}_{lmn}^-$ in (2.11).

### E. Significance of the EMRI fluxes and of their PN expansions

The two fluxes (2.19) and (2.20), along with the additional pair at the larger black hole's horizon, are critical to our understanding and description of EMRI radiation. It has been shown through the use of multiple timescale analysis that these first-order, orbit-averaged fluxes form the dominant contribution to the system's cumulative phase [83,106]. This phase must be known to within a fraction of a radian over the inspiral's lifetime for the successful detection and characterization of EMRIs by LISA [1].

Within the multiscale framework, the exclusive use of the fluxes to model EMRIs is known as the adiabatic approximation. Such an approach has been used to simulate EMRIs and generate coarse but efficient waveforms across various realms of parameter space [44,107–110]. However, it is known that adiabatic waveforms will be insufficient for EMRI parameter estimation with LISA, which will require knowledge of all contributions through post-1 adiabatic

order, including resonance effects, the oscillatory first-order self-force, and the second-order fluxes [83,106].

Nevertheless, as the leading contribution, the first-order fluxes must be known to significantly higher accuracy than the other quantities, all of which appear in the cumulative phase at higher order in the mass ratio. As a result, there has been a great deal of past work analyzing the total energy and angular momentum radiated by EMRIs. The primary approach to flux determination has historically been direct numerical calculation (e.g., [109,111]). Large swaths of numeric flux computations can be combined with suitable interpolation schemes to obtain accurate expressions across parameter space, which can then be used to simulate the inspiral [84].

Low-order analytic PN expansions of the flux formulas (2.19) and (2.20) using the MST solutions have also been known quite some time [112]. These have been useful for verifying numerical calculations, informing PN theory, and generating rapid inspiral simulations. However, because they lose accuracy near the point of merger, it was generally thought that their utility in the generation of full waveform templates would be limited.

More recently, there have been a number of discoveries on the accuracy of high-order BHPT-PN expansions which have led to increased confidence in their relevance in the strong-field regime. In particular, it was shown directly in the plast decade that high-PN-order expansions in many cases converge (albeit slowly) all the way to the orbit's separatrix, if not its light ring. This was first demonstrated for the energy flux at infinity in 2012 for the case of circular orbits about a Schwarzschild background [43,44]. There, the author found that 22PN expressions were able to match numerical adiabatic simulations all the way to the innermost stable circular orbit (ISCO). Similar results have been obtained for high-order expansions of certain conservative-sector quantities, again for the case of circular orbits on a Schwarzschild background [48,50,57].

It has also been found that the use of factorization schemes or resummation methods can improve the convergence of these expansions even further [59,71,82,90]. For instance, as proposed in [113], the simple process of reexpanding the logarithm of the $lm$ (circular-orbit) mode fluxes, evaluating numerically, and then exponentiating the result often improves agreement with numerical calculations at the ISCO [90]. Resummed high-order BHPT-PN expansions are especially well suited to the development of EOB waveforms, which have thus far been highly successful at simulating binaries across large regions of parameter space [35–37,71,114–120].

Still, the convergence properties of the expansions and overall utility of this approach in more intricate EMRIs remain an open question of study, though progress has been made. The energy flux series for circular, equatorial orbits on a Kerr background was derived to 11PN in [82], and this was found to agree with numerical calculations up to velocities of about 0.4 for both prograde and retrograde orbits [60,121]. In the case of fully generic orbits on a Kerr background, series are presently published only to 4PN and $e^6$, and the strong-field behavior is unknown [52]. Results that incorporate secondary spin have also been published in [122] with some analysis of strong-field convergence.

The present work focuses on high-order flux expansions for eccentric orbits on a Schwarzschild background, offering a necessary intermediate step on the path to fully generic orbits. The convergence properties of the expansions can be analyzed, both with and without the use of basic resummation methods, allowing for comparison to the circular-orbit results of [44,60,82,121]. We will find that the convergence worsens with increasing $e$, but there will still be large regions of parameter space where the high-order expansions are useful.

## III. ANALYTIC EXPANSION OF THE MST HOMOGENEOUS SOLUTIONS

The previous section offered a broad overview of the techniques that will be used to compute the two fluxes at infinity for eccentric-orbit inspirals. Now we move to the specific implementation used to construct our high-order PN expansions. This section will detail the process of expanding the odd-parity MST homogeneous solutions, generally following the prescription detailed in [50], which was based on the original analytic expansion methods developed in [78,79]. The next section will then cover the inhomogeneous integral and source motion.

To begin, the odd-parity infinity- and horizon-side MST homogeneous solutions can be written as [50,77,100]

$$X^{+}_{lmn} = e^{iz} z^{\nu+1} \left(1-\frac{\epsilon}{z}\right)^{-i\epsilon} \sum_{j=-\infty}^{\infty} a_j (-2iz)^j \frac{\Gamma(j+\nu+1-i\epsilon)\Gamma(j+\nu-1-i\epsilon)}{\Gamma(j+\nu+3+i\epsilon)\Gamma(j+\nu+1+i\epsilon)} \times U(j+\nu+1-i\epsilon, 2j+2\nu+2, -2iz), \tag{3.1}$$

$$X^{-}_{lmn} = e^{-iz} \left(\frac{z}{\epsilon}-1\right)^{-i\epsilon} \left(\frac{\epsilon}{z}\right)^{i\epsilon+1} \sum_{j=-\infty}^{\infty} a_j \frac{\Gamma(j+\nu-1-i\epsilon)\Gamma(-j-\nu-2-i\epsilon)}{\Gamma(1-2i\epsilon)} \times {}_2F_1(j+\nu-1-i\epsilon, -j-\nu-2-i\epsilon; 1-2i\epsilon; 1-z/\epsilon). \tag{3.2}$$

In these expressions, $\nu = \nu(l,\epsilon)$ is the renormalized angular momentum, a special parameter chosen to make the summations converge (see [77,100]), and $a_j = a_j(l,\epsilon)$ are $\nu$-dependent series coefficients. $U(a,b,\zeta)$ is the irregular confluent hypergeometric function, and ${}_2F_1(a,b,c,\zeta)$ is the hypergeometric function. Finally, $\epsilon = 2M\omega\eta^3$ and $z = r\omega\eta$, with $\eta = 1/c$, serve as the expansion parameters. (In this section, factors of $c$ are restored to track PN order.)

Everything contained within $X^+_{lmn}$ and $X^-_{lmn}$ depends upon $\epsilon$ and $z$ and thus on $\eta$. By definition $\eta^2$ corresponds to 1PN order. Therefore, both $X^+_{lmn}$ and $X^-_{lmn}$ can be directly expanded in $\eta$ analytically, and this is achieved here to high order using the algebraic computing software *Mathematica*. Note briefly that the MST solutions presented above are slightly different from those given in [50,77,100]. Here, we have preemptively canceled a few $z$-independent factors that do not contribute to the radiation.

### A. Expansion of $\nu$ and $a_j$

The PN expansion procedure is best begun with renormalized angular momentum $\nu$ and series coefficients $a_j$, which identically appear in both $X^+_{lmn}$ and $X^-_{lmn}$. These terms are computed via the resolution of a continued fraction equation, defined to make the sum converge as $j \to \pm\infty$. This equation is given by [100]

$$\alpha_j a_{j+1} + \beta_j a_j + \gamma_j a_{j-1} = 0, \tag{3.3}$$

with

$$\begin{aligned}
\alpha_j &= -\frac{i\epsilon(-1-i\epsilon+j+\nu)(-1+i\epsilon+j+\nu)(1-i\epsilon+j+\nu)}{(1+j+\nu)(3+2j+2\nu)},\\
\beta_j &= 2\epsilon^2 - l(l+1) + \frac{\epsilon^2(\epsilon^2+4)}{(j+\nu)(1+j+\nu)} + (j+\nu)(1+j+\nu),\\
\gamma_j &= \frac{i\epsilon(i\epsilon+j+\nu)(2-i\epsilon+j+\nu)(2+i\epsilon+j+\nu)}{(j+\nu)(-1+2j+2\nu)}.
\end{aligned} \tag{3.4}$$

This is solved to some desired power of $\epsilon$ by setting

$$\alpha_j R_{j+1} + \beta_j + \gamma_j L_{j-1} = 0, \tag{3.5}$$

where $R$ and $L$ are the continued fractions:

$$\begin{aligned}
R_{j+1} &= \frac{a_{j+1}}{a_j} = -\frac{\gamma_{j+1}}{\beta_{j+1}-}\frac{\alpha_{j+1}\gamma_{j+2}}{\beta_{j+2}-}\frac{\alpha_{j+2}\gamma_{j+3}}{\beta_{j+3}-\cdots},\\
L_{j-1} &= \frac{a_{j-1}}{a_j} = -\frac{\alpha_{j-1}}{\beta_{j-1}-}\frac{\gamma_{j-1}\alpha_{j-2}}{\beta_{j-2}-}\frac{\gamma_{j-2}\alpha_{j-3}}{\beta_{j+3}-\cdots}.
\end{aligned} \tag{3.6}$$

First, $\nu$ is found to some given order in $\epsilon$ by fixing $j$ and truncating the fractions at the needed depth. An ansatz of $\nu = \nu_0 + \nu_2\epsilon^2 + \nu_4\epsilon^4\cdots$ can be substituted, and the resulting equation can be solved order by order to extract each $\nu_i$ [123]. Then, the series coefficients $a_j$ can be iteratively built up using $a_{j+1} = R_{j+1}a_j$ and $a_{j-1} = L_{j-1}a_j$.

As an example, $\nu$ and some of the series coefficients for $l = 2$ can be found as [123]

$$\begin{aligned}
\nu = 2 &- \frac{107\epsilon^2}{210} - \frac{1695233\epsilon^4}{9261000} - \frac{76720109901233\epsilon^6}{480698687700000}\\
&- \frac{71638806585865707261481\epsilon^8}{389235629236738284000000} + \mathcal{O}(\epsilon^{10}),
\end{aligned} \tag{3.7}$$

$$\begin{aligned}
a_{-4} &= -\frac{7i\epsilon^5}{856} - \frac{53\epsilon^6}{6420} + \mathcal{O}(\epsilon^7),\\
a_{-3} &= -\frac{7\epsilon^4}{1926} + \frac{211i\epsilon^5}{28890} - \frac{3985481\epsilon^6}{370947600} + \mathcal{O}(\epsilon^7),\\
a_{-2} &= \frac{11\epsilon^4}{12840} - \frac{11i\epsilon^5}{8560} + \frac{18652901\epsilon^6}{15147027000} + \mathcal{O}(\epsilon^7),\\
a_{-1} &= -\frac{i\epsilon^3}{20} - \frac{\epsilon^4}{40} - \frac{4920329i\epsilon^5}{94374000} - \frac{3061237\epsilon^6}{94374000} + \mathcal{O}(\epsilon^7),\\
a_0 &= 1,\\
a_1 &= -\frac{5i\epsilon}{6} + \frac{5\epsilon^2}{18} - \frac{12029i\epsilon^3}{52920} + \frac{19519\epsilon^4}{158760}\\
&\quad - \frac{4807626493i\epsilon^5}{25671492000} + \frac{2573708771\epsilon^6}{25671492000} + \mathcal{O}(\epsilon^7),\\
a_2 &= -\frac{15\epsilon^2}{49} - \frac{5i\epsilon^3}{28} - \frac{730781\epsilon^4}{6338640} - \frac{2691i\epsilon^5}{24640}\\
&\quad - \frac{921715511273\epsilon^6}{8882970096000} + \mathcal{O}(\epsilon^7),\\
a_3 &= \frac{5i\epsilon^3}{72} - \frac{47\epsilon^4}{864} + \frac{1379137i\epsilon^5}{49533120} - \frac{58088509\epsilon^6}{1485993600} + \mathcal{O}(\epsilon^7),\\
a_4 &= \frac{10\epsilon^4}{891} + \frac{19i\epsilon^5}{1782} + \frac{8914057\epsilon^6}{2074675680} + \mathcal{O}(\epsilon^7).
\end{aligned} \tag{3.8}$$

As we can see, the results for negative $j$ are not quite regular. This is due to the fact that $L_j$ experiences cancellation in its denominator for certain values of $j < 0$. Thus, the corresponding $L_j$ either gains or loses additional powers of $\epsilon$. Fortunately, this behavior can be precisely determined, and the starting orders are listed in [50].

### B. Expansion of the infinity-side homogeneous solution $X^+_{lmn}$

The remaining factors in the homogeneous solutions have additional subtleties that complicate their expansions. A complete description of the process was provided in [50]; therefore, our treatment here will be brief. We start with the odd-parity solution $X^+_{lmn}$ in (3.1). This function is most easily expanded in a few separate pieces, which can then be combined with $\nu$ and the $a_j$ to produce the full solution.

### 1. The initial prefactor, $C_{\rm up}$

First, the expansion of the prefactor is straightforward. We slightly modify the expansion variables and write

$$C_{\rm up} = e^{iz} z^{\nu+1} \left(1 - \frac{\epsilon}{z}\right)^{-i\epsilon} = e^{i\bar{z}\eta} (\bar{z}\eta)^{\nu+1} \left(1 - \frac{\bar{\epsilon}}{\bar{z}}\eta^2\right)^{-i\bar{\epsilon}\eta^3}, \tag{3.9}$$

where we have defined $\bar{z} = r\omega$ and $\bar{\epsilon} = 2M\omega$. Thus, $z = \bar{z}\eta, \epsilon = \bar{\epsilon}\eta^3$, which allows for straightforward expansion in $\eta$. This substitution can be utilized throughout the procedure to more easily track powers of $\eta$. Note that the factor of $z^{\nu+1}$ ensures that $C_{\rm up}$ will begin at order $\mathcal{O}(\eta^{l+1})$. As an example, this can be found for $l = 2$ to give

$$C_{\rm up}^{l=2} = \bar{z}^3\eta^3 + i\bar{z}^4\eta^4 - \frac{\bar{z}^5}{2}\eta^5 - \frac{1}{6}i\bar{z}^6\eta^6 + \frac{\bar{z}^7}{24}\eta^7 + \left(i\bar{\epsilon}^2\bar{z}^2 + \frac{i\bar{z}^8}{120}\right)\eta^8 - \left(\bar{\epsilon}^2\bar{z}^3 + \frac{\bar{z}^9}{720} + \frac{107}{210}\bar{\epsilon}^2\bar{z}^3\log(\bar{z}\eta)\right)\eta^9 + \mathcal{O}(\eta^{10}). \tag{3.10}$$

### 2. Manipulation of the hypergeometric function

The primary remaining complication is the irregular confluent hypergeometric function $U$, which must be recast using hypergeometric identities into a form more suitable for PN expansion. One useful choice is

$$U(a,b,\zeta) = \frac{\Gamma(1-b)}{\Gamma(a-b+1)} M(a,b,\zeta) + \frac{\Gamma(b-1)}{\Gamma(a)} \zeta^{1-b} M(a-b+1, 2-b, \zeta) \tag{3.11}$$

for Kummer hypergeometric function $M(a,b,\zeta) = {}_1F_1(a,b,\zeta)$ [50].

Taking the two instances of $M$ separately, and including the other factors in the summation for $X^+_{lmn}$, the first portion can be written as

$$U_1^{lj} \equiv (-2iz)^j \frac{\Gamma(j+\nu-1-i\epsilon)\Gamma(j+\nu+1-i\epsilon)\Gamma(-2j-2\nu-1)}{\Gamma(j+\nu+3+i\epsilon)\Gamma(j+\nu+1+i\epsilon)\Gamma(-j-\nu-i\epsilon)} M(j+\nu+1-i\epsilon, 2j+2\nu+2, -2iz). \tag{3.12}$$

The function $U_1^{lj}$ exhibits PN irregularities in both the $\Gamma$ prefactors and the function $M$. In the product of $\Gamma$ functions, factors of $\epsilon$ are lost whenever a term in the numerator has an argument $\leq 0$, and they are gained whenever a term in the denominator has an argument $\leq 0$. Once this is accounted for, the $\Gamma$ product can be properly expanded to any order in $\epsilon$, though the basic execution in *Mathematica* can be slow.

For $M(j+\nu+1-i\epsilon, 2j+2\nu+2, -2iz)$, irregular behavior occurs when $j + l < 0$. This can be observed in the hypergeometric series:

$$M(a,b,z) = \sum_{k=0}^{\infty} \frac{(a)_k}{(b)_k} \frac{z^k}{k!}, \qquad (a)_k = \frac{\Gamma(a+k)}{\Gamma(a)} = (a)(a+1)(a+2)\cdots(a+k-1), \tag{3.13}$$

where $(a)_k$ is the Pochhammer symbol. Thus, when $j+l=-1$, the PN series for $M(j+\nu+1-i\epsilon, 2j+2\nu+2, -2iz)$ starts at $\mathcal{O}(1/\eta^2)$.

The second piece, given by

$$U_2^{lj} = (-2iz)^{(-j-2\nu-1)} \frac{\Gamma(j+\nu-1-i\epsilon)\Gamma(2j+2\nu+1)}{\Gamma(j+\nu+3+i\epsilon)\Gamma(j+\nu+1+i\epsilon)} \times M(-j-\nu-i\epsilon, -2j-2\nu, -2iz), \tag{3.14}$$

is handled similarly.

### 3. The full $X^+_{lmn}$

The full expansion of $X^+_{lmn}$ proceeds by combining the series for these component pieces. Within the summation series must be computed for all $j$ whose leading order is below the target order of the full expansion. To aid this effort, Table I establishes the leading PN orders of $X^+_{lmn}$ for

TABLE I. Leading powers of $\eta$ in $C_{\rm up} a_j U_1^{lj}$ and $C_{\rm up} a_j U_2^{lj}$ as functions of $l$ and $j$.

| | $j \leq -2l-1$ | $-2l \leq j \leq -l-3$ | $-l-2 \leq j \leq -l-1$ | $-l \leq j \leq -l+1$ | $j \geq -l+2$ |
|---|---|---|---|---|---|
| $C_{\rm up} a_j U_1^{lj}$ | $2\lvert j\rvert + l - 2$ | $2\lvert j\rvert + l + 4$ | $3\lvert j\rvert - j - l - 3$ | $3\lvert j\rvert + j + l + 1$ | $3\lvert j\rvert + j + l - 2$ |
| $C_{\rm up} a_j U_2^{lj}$ | $4\lvert j\rvert - l - 6$ | $4\lvert j\rvert - l$ | $3\lvert j\rvert - j - l - 3$ | $3\lvert j\rvert + j + l + 1$ | $3\lvert j\rvert - j - l$ |

each $l$ and $j$. An equivalent table is given in [50]. In this way it can be determined how many $j$ values must be retained for a given $l$ to reach any desired order. For example, in order to calculate $X^{+}_{2mn}$ to, say, $\eta^4$, we must include $0 \le j \le 1$ for $U_1^{2j}$ and $0 \le j \le 3$ for $U_2^{2j}$. A low-order expansion for the normalized version of $X^{+}_{2mn}$ will be shown in Sec. III D.

### C. Expansion of the horizon solution $X^{-}_{lmn}$

#### 1. Separating and expanding the hypergeometric function

The prefactor $C_{\rm in} = e^{-iz}\left(\frac{z}{\epsilon}-1\right)^{-i\epsilon}\left(\frac{\epsilon}{z}\right)^{i\epsilon+1}$ is expanded similarly to its infinity-side counterpart. The hypergeometric function ${}_2F_1(a,b,c,\zeta)$, meanwhile, can be separated into a form more amenable to the present expansion [50]:

$$
\begin{aligned}
{}_2F_1(a,b,c,\zeta) = {} & \frac{\Gamma(c)\Gamma(b-a)}{\Gamma(b)\Gamma(c-a)}(1-\zeta)^{-a}\,{}_2F_1\left(a,c-b,a-b+1,\frac{1}{1-\zeta}\right) \\
& + \frac{\Gamma(c)\Gamma(a-b)}{\Gamma(a)\Gamma(c-b)}(1-\zeta)^{-b}\,{}_2F_1\left(c-a,b,b-a+1,\frac{1}{1-\zeta}\right).
\end{aligned} \tag{3.15}
$$

The first appearance ${}_2F_1$ can be combined with remaining factors in the summand to produce the function

$$
F_1^{lj} = \frac{\Gamma(j+\nu-1-i\epsilon)\Gamma(-2j-2\nu-1)}{\Gamma(-j-\nu-i\epsilon+2)}\left(\frac{\epsilon}{z}\right)^{j+\nu-1-i\epsilon}{}_2F_1(j+\nu-1-i\epsilon, j+\nu+3-i\epsilon, 2j+2\nu+2, \epsilon/z). \tag{3.16}
$$

Once again, irregularities in leading PN order exist in the $\Gamma$ functions and in ${}_2F_1(j+\nu-1-i\epsilon, j+\nu+3-i\epsilon, 2j+2\nu+2, \epsilon/z)$ itself. For ${}_2F_1(j+\nu-1-i\epsilon, j+\nu+3-i\epsilon, 2j+2\nu+2, \epsilon/z)$, irregular behavior occurs when the various arguments are nonpositive, as can be observed from the hypergeometric series:

$$
{}_2F_1(a,b;c;z) = \sum_{k=0}^{\infty}\frac{(a)_k(b)_k}{(c)_k}\frac{z^k}{k!}. \tag{3.17}
$$

The series will start at $\mathcal{O}(\eta^{-4})$ for $j=-l-1$ and at $\mathcal{O}(1)$ otherwise.

The second appearance of ${}_2F_1$ is combined with its multiplicative factors to yield a second function:

$$
\begin{aligned}
F_2^{lj} = {} & \frac{\Gamma(-j-\nu-2-i\epsilon)\Gamma(2j+2\nu+1)}{\Gamma(j+\nu-i\epsilon+3)}\left(\frac{\epsilon}{z}\right)^{-j-\nu-2-i\epsilon} \\
& \times {}_2F_1(-j-\nu+2-i\epsilon, -j-\nu-2-i\epsilon, -2j-2\nu, \epsilon/z).
\end{aligned} \tag{3.18}
$$

The hypergeometric function here has leading behavior of $\mathcal{O}(\eta^{-4})$ for $j=-l$ and of $\mathcal{O}(1)$ otherwise.

#### 2. The full horizon-side homogeneous solution

The computation of $X^{-}_{lmn}$ follows from these component pieces. The combined leading behavior is given in Table II. Note that this corrects a few small mistakes in Table III of [50]. Thus, calculation of $X^{-}_{2mn}$ to, say, $1/\eta$, requires no $j$ for $F_1^{2j}$ and $0 \le n \le 8$ for $F_2^{2j}$. An expansion for a normalized version of $X^{-}_{2mn}$ will be given in Sec. III D below.

### D. The normalized functions, $\hat{X}^{+}_{lmn}$ and $\hat{X}^{-}_{lmn}$

The functions $X^{\pm}_{lmn}$ will each have some amplitude at infinity or the horizon $X^{\pm}_{lmn} \sim A^{\pm}_{lmn}e^{\pm iwr_*}$, $r_* \to \pm\infty$, where $r_* = r + 2M\ln(r/2M-1)$ is the tortoise coordinate. As mentioned in Sec. II, it is advantageous in the computation of the fluxes to normalize these functions so that we have $\hat{X}^{\pm}_{lmn} \sim e^{\pm iwr_*}$ as $r \to \infty$ or $r \to 2M$. This is done by dividing off the initial amplitudes $A^{\pm}_{lmn}$, found by analyzing the appropriate limits.

Explicitly, the function $X^{+}_{lmn}$ can be normalized by taking the limit $r \to \infty$ or, equivalently, $z \to \infty$. Noting that $U(a,b,z)$ limits to $z^{-a}$ as $z \to \infty$, we find that the desired amplitude is given by

TABLE II. Leading powers of $\eta$ in $C_{\rm in}a_jF_1^{lj}$ and $C_{\rm in}a_jF_2^{lj}$ as functions of $l$ and $j$.

| | $j \le -2l-1$ | $-2l \le j \le -l-3$ | $j=-l-2$ | $-l-1 \le j \le -l$ | $j=-l+1$ | $j \ge -l+2$ |
|---|---|---|---|---|---|---|
| $C_{\rm in}a_jF_1^{lj}$ | $\lvert j\rvert+2l-6$ | $\lvert j\rvert+2l$ | $3\lvert j\rvert-4$ | $3l-3$ | $3\lvert j\rvert-1$ | $3\lvert j\rvert+2j+2l-3$ |
| $C_{\rm in}a_jF_2^{lj}$ | $5\lvert j\rvert-2l-8$ | $5\lvert j\rvert-2l-2$ | $3\lvert j\rvert-4$ | $3l-3$ | $3\lvert j\rvert-1$ | $3\lvert j\rvert-2j-2l-5$ |

TABLE III. Overview of the computational time needed for expansion of various even-parity normalization constants to high PN order. Expansions were found for specific $l$ but general $m$ and $n$ on the UNC Longleaf cluster. The third and fourth columns indicate the time and memory, respectively, needed for the calculation. The fifth column gives the approximate size of a text file holding the output. In each case the comparable odd-parity computation is simpler and faster. Note that only the infinity-side coefficients are needed for the fluxes at infinity. Radiation to the larger black hole's horizon will be explored in a future paper [128].

| Coefficient | Relative order | CPU time [hours] | Memory | Text file size |
|---|---|---|---|---|
| $C^+_{2mn}$ | $19\mathrm{PN}/e^{10}$ | 173.5 | 5 GB | 60 MB |
| $C^+_{4mn}$ | $18\mathrm{PN}/e^{10}$ | 41.1 | 4 GB | 15 MB |
| $C^+_{6mn}$ | $16\mathrm{PN}/e^{10}$ | 18.1 | 4 GB | 10 MB |
| $C^+_{2mn}$ | $10\mathrm{PN}/e^{20}$ | 8.2 | 3 GB | 40 MB |

$$\begin{aligned} A^+_{lmn} &= (\epsilon)^{i\epsilon}(-2i)^{-\nu-1+i\epsilon}\sum_{j=-\infty} a_j \frac{\Gamma(j+\nu-1-i\epsilon)\Gamma(j+\nu+1-i\epsilon)}{\Gamma(j+\nu+3+i\epsilon)\Gamma(j+\nu+1+i\epsilon)} \\ &= (\epsilon)^{i\epsilon}(-2i)^{-\nu-1+i\epsilon}A^{\mathrm{sum}}_{\mathrm{up}}. \end{aligned} \tag{3.19}$$

$\hat{X}^+_{lmn}$ follows by dividing off this amplitude. Absorbing the amplitude into the prefactor, we find

$$\hat{C}_{\mathrm{up}} = \frac{C_{\mathrm{up}}}{A^+_{lmn}} = \frac{e^{iz}(-2iz)^{\nu+1}}{A^{\mathrm{sum}}_{\mathrm{up}}}(-2i\epsilon)^{-i\epsilon}\left(1-\frac{\epsilon}{z}\right)^{-i\epsilon}.$$

For $l=2$ the expansion for the full normalized homogeneous solution begins as

$$\begin{aligned} \hat{X}^+_{2mn} = &-\frac{3}{\bar{z}^2\eta^2} - \left(\frac{1}{2}+\frac{5\bar{\epsilon}}{2\bar{z}^3}\right) + \left(-\frac{5i\bar{\epsilon}}{\bar{z}^2}+\frac{3i\bar{\epsilon}\gamma}{\bar{z}^2}+\frac{3\bar{\epsilon}\pi}{2\bar{z}^2}+\frac{3i\bar{\epsilon}}{\bar{z}^2}\log(2\bar{\epsilon}\eta^3)\right)\eta + \left(-\frac{15\bar{\epsilon}^2}{7\bar{z}^4}-\frac{7\bar{\epsilon}}{4\bar{z}}-\frac{\bar{z}^2}{8}\right)\eta^2 \\ &+\left(-\frac{5i\bar{\epsilon}}{6}+\frac{i\bar{\epsilon}\gamma}{2}+\frac{\bar{\epsilon}\pi}{4}-\frac{25i\bar{\epsilon}^2}{6\bar{z}^3}+\frac{5i\bar{\epsilon}^2\gamma}{2\bar{z}^3}+\frac{5\bar{\epsilon}^2\pi}{4\bar{z}^3}-\frac{i\bar{z}^3}{15}+\frac{1}{2}i\bar{\epsilon}\log(2\bar{\epsilon}\eta^3)+\frac{5i\bar{\epsilon}^2}{2\bar{z}^3}\log(2\bar{\epsilon}\eta^3)\right)\eta^3 \\ &+\left(-\frac{15\bar{\epsilon}^3}{8\bar{z}^5}+\frac{3757\bar{\epsilon}^2}{420\bar{z}^2}-\frac{457\bar{\epsilon}^2\gamma}{70\bar{z}^2}+\frac{3\bar{\epsilon}^2\gamma^2}{2\bar{z}^2}+\frac{457i\bar{\epsilon}^2\pi}{140\bar{z}^2}-\frac{3i\bar{\epsilon}^2\gamma\pi}{2\bar{z}^2}-\frac{5\bar{\epsilon}^2\pi^2}{8\bar{z}^2}-\frac{7\bar{\epsilon}\,\bar{z}}{16}+\frac{\bar{z}^4}{48}-\frac{5\bar{\epsilon}^2}{\bar{z}^2}\log(2\bar{\epsilon}\eta^3)\right. \\ &\left.+\frac{3\bar{\epsilon}^2\gamma}{\bar{z}^2}\log(2\bar{\epsilon}\eta^3)-\frac{3i\bar{\epsilon}^2\pi}{2\bar{z}^2}\log(2\bar{\epsilon}\eta^3)+\frac{3\bar{\epsilon}^2}{2\bar{z}^2}\log^2(2\bar{\epsilon}\eta^3)-\frac{107\bar{\epsilon}^2}{70\bar{z}^2}\log(2\bar{z}\eta)\right)\eta^4+\mathcal{O}(\eta^5). \end{aligned} \tag{3.20}$$

The function $\hat{X}^-_{lmn}$, meanwhile, is normalized by taking the limit $r\to 2M$, which implies $z\to\epsilon$. Because ${}_2F_1(a,b,c,1-r/2M)$ limits to 1 as $r\to 2M$ for any $(a,b,c)$, we find the amplitude

$$A^-_{lmn} = \sum_{n=-\infty} a_j \frac{\Gamma(n+\nu-1-i\epsilon)\Gamma(-n-\nu-2-i\epsilon)}{\Gamma(1-2i\epsilon)}. \tag{3.21}$$

$\hat{X}^-_{lmn}$ follows by dividing off this amplitude. The series for $l=2$ is found to be

$$\begin{aligned} \hat{X}^-_{2mn} = &\frac{\bar{z}^3}{\bar{\epsilon}^3\eta^6}-\frac{\bar{z}^5}{14\bar{\epsilon}^3\eta^4}+\frac{13i\bar{z}^3}{12\bar{\epsilon}^2\eta^3}+\left(-\frac{13\bar{z}^4}{42\bar{\epsilon}^2}+\frac{\bar{z}^7}{504\bar{\epsilon}^3}\right)\frac{1}{\eta^2}-\frac{13i\bar{z}^5}{168\bar{\epsilon}^2\eta} \\ &+\left(-\frac{95\bar{z}^3}{48\bar{\epsilon}}-\frac{\pi^2\bar{z}^3}{6\bar{\epsilon}}+\frac{\bar{z}^6}{54\bar{\epsilon}^2}-\frac{\bar{z}^9}{33264\bar{\epsilon}^3}+\frac{107\bar{z}^3}{210\bar{\epsilon}}\log\left(\frac{\bar{\epsilon}}{\bar{z}}\eta^2\right)\right)+\left(-\frac{169i\bar{z}^4}{504\bar{\epsilon}}+\frac{13i\bar{z}^7}{6048\bar{\epsilon}^2}\right)\eta \\ &+\left(\frac{319\bar{z}^2}{420}+\frac{85429\bar{z}^5}{493920\bar{\epsilon}}+\frac{\pi^2\bar{z}^5}{84\bar{\epsilon}}-\frac{53\bar{z}^8}{118800\bar{\epsilon}^2}+\frac{\bar{z}^{11}}{3459456\bar{\epsilon}^3}-\frac{107\bar{z}^5}{2940\bar{\epsilon}}\log\left(\frac{\bar{\epsilon}}{\bar{z}}\eta^2\right)\right)\eta^2+\mathcal{O}(\eta^3). \end{aligned} \tag{3.22}$$

### E. Optimizing expansions through Γ function identities and factorization

#### 1. Rewriting Γ functions using Pochhammer symbols

The procedure detailed above is sufficient to produce PN series; however, the expressions are too computationally expensive as written, primarily due to the complexity of the Γ functions, which are difficult to expand when the arguments are arbitrary. Fortunately, it is possible to reformulate the Γ functions slightly to construct series in a much more efficient manner. This is done by first repeatedly applying the standard identity $z\Gamma(z) = \Gamma(z+1)$ to put all such functions into the form $\Gamma(1+g(\epsilon))$ for some small function $g(\epsilon)$ and then, because the resulting $\Gamma(1+g(\epsilon))$ expressions can be pulled out of the summations over $j$, finding opportunities to cancel or simplify these factors.

Explicitly, we write

$$\begin{aligned}\Gamma(k+g(\epsilon)) &= \Gamma(1+g(\epsilon))\left(\frac{\Gamma(k+g(\epsilon))}{\Gamma(1+g(\epsilon))}\right)\\ &= \Gamma(1+g(\epsilon))(1+g(\epsilon))_{k-1},\end{aligned} \tag{3.23}$$

where $k \neq 1$ is some integer and $(a)_n$ is the Pochhammer symbol. In this context, the Pochhammer symbol takes one of two values, depending on the value of $k$:

$$\begin{aligned}(1+g(\epsilon))_{k-1} &= \prod_{i=1}^{k-1}(i+g(\epsilon))(k>1),\\ (1+g(\epsilon))_{k-1} &= \prod_{i=k}^{0}\left(\frac{1}{i+g(\epsilon)}\right)(k<1).\end{aligned} \tag{3.24}$$

In each case, this yields a purely rational series in $\epsilon$, one which can be rapidly expanded in *Mathematica*. Doing this for each Γ function in $\hat{X}^{+}_{lmn}$ and $\hat{X}^{-}_{lmn}$ creates significant cancellations of Γ functions in $A^{\pm}_{lmn}$ with those in $U^{lj}_1, U^{lj}_2, F^{lj}_1, F^{lj}_2$ drastically reducing the computational cost. In what follows, we will call the functions that remain after such cancellations $\bar{U}^{lj}_1, \bar{U}^{lj}_2, \bar{F}^{lj}_1, \bar{F}^{lj}_2$, respectively.

#### 2. Factorization

We can simplify $\hat{X}^{\pm}_{lmn}$ further by preemptively factoring out certain complicated $z$-independent terms. In certain cases these factors will eventually cancel through division by the Wronskian [50], but the rest of the time, we will simply multiply these factors back in at the end, after $|C^{\pm}_{lmn}|^2$ is constructed for the fluxes. This serves to accelerate the integral for the normalization coefficients $C^{\pm}_{lmn}$ (the rate-limiting step in the expansion of the fluxes) by an order of magnitude.

To give an immediate example, the expression for $\hat{X}^{+}_{lmn}$ contains the $z$-independent factor

$$(-2i\epsilon)^{-i\epsilon} = \exp\left[-i\epsilon\log(-2i\epsilon)\right]. \tag{3.25}$$

This piece expands into a sequence of logarithms that greatly increases the expression length and computational cost. Therefore, this factor is removed from the outset.

More subtly, we can simplify the summations in $X^{-}_{lmn}$ and $X^{+}_{lmn}$ by analyzing more closely the leading behavior of the functions $\bar{U}^{lj}_1, \bar{U}^{lj}_2, \bar{F}^{lj}_1, \bar{F}^{lj}_2$. On the horizon side, multiplying in the $(\epsilon/z)^{i\epsilon+1}$ factor from $C_{\rm in}$, we have

$$\begin{aligned}\left(\frac{\epsilon}{z}\right)^{i\epsilon+1}\bar{F}^{lj}_1 &\propto \left(\frac{\epsilon}{z}\right)^{j+\nu},\\ \left(\frac{\epsilon}{z}\right)^{i\epsilon+1}\bar{F}^{lj}_2 &\propto \left(\frac{\epsilon}{z}\right)^{-j-\nu-1}.\end{aligned} \tag{3.26}$$

Note that the latter expression controls the leading behavior [$(z/\epsilon)^{l+1}$ for $j=0$], while the former holds an additional factor of $(\epsilon/z)^{2l+1} \propto \eta^{4l+2}$. Therefore, when attempting to reach a given PN order, expansions of $\bar{F}^{lj}_2$ must be computed for more $j$ and to higher relative order than for those of $\bar{F}^{lj}_1$.

Similarly, in $X^{+}_{lmn}$, $\bar{U}^{lj}_2$ has an extra factor of $(z^{-l})$ over $\bar{U}^{lj}_1$, though the difference there is more modest. Because the $\bar{F}^{lj}_1$ and $\bar{U}^{lj}_1$ calculations are simpler and fewer in number, we can reduce the total computations by "moving" all the $j$-independent $\Gamma(1+g(\epsilon))$ functions from $\bar{F}^{lj}_2$ and $\bar{U}^{lj}_2$ to $\bar{F}^{lj}_1$ and $\bar{U}^{lj}_1$ via division. When necessary, these factors will be multiplied back in at the end [90].

Finally, it is possible to identify one additional simplifying factor: the lowest appearance of each Euler log–like function [48,72,87,90,115]. These functions are produced by the leading-order behavior within $\hat{U}_2$ and $\hat{F}_2$ [90]. Upon evaluation at the location of the particle (see Sec. IV below), this adduces the factors

$$\begin{aligned}X^{+}_{lmn} &: (-i\epsilon p)^{-\Delta\nu},\\ X^{-}_{lmn} &: \left(\frac{2}{p}\right)^{-\Delta\nu},\end{aligned} \tag{3.27}$$

where $\Delta\nu = \nu - l$.

Once all such quantities are canceled or factored out of the homogeneous solutions, the resulting expansions are multiple orders of magnitude simpler and faster to execute. However, when constructed in this manner, the $X^{\pm}_{lmn}$ functions are no longer normalized, so we no longer mark them with hats. The missing factors will eventually be resupplied in the final construction of the fluxes. They are given explicitly in Sec. IV.

### F. The functions $\hat{X}^{\rm e}_{\rm up}$ and $\hat{X}^{\rm e}_{\rm in}$ (even parity)

The even-parity functions can be found by using the Detweiler-Chandrasekar transformation [101–104],

$$X_{\pm}^{\rm even} = \left(\frac{4}{\lambda_l \pm 6i\epsilon}\right)\left[\frac{3\epsilon}{2}\left(1-\frac{\epsilon}{z}\right)\frac{dX_{\pm}^{\rm odd}}{dz} + \left(\frac{1}{4}\lambda_l + \frac{9\epsilon^2(1-\frac{\epsilon}{z})}{2(l-1)(l+2)z^2+6z\epsilon}\right)X_{\pm}^{\rm odd}\right], \quad (3.28)$$

where $\lambda_l = (l-1)l(l+1)(l+2)$. This transformation is constructed such that whenever the odd-parity functions are normalized, the even-parity ones will be as well. This can be checked directly by taking the appropriate limits. Thus, the bulk of the expansion procedure remains unchanged in the even-parity case.

## IV. ANALYTIC EXPANSION OF THE NORMALIZATION CONSTANTS

### A. Obtaining PN series for the geodesic motion of the smaller body

The prescription above allows for expansion of the homogeneous solutions to effectively arbitrary PN order. These can be used to construct the normalization constants $C_{lmn}^{\pm}$ defined in Sec. II B. To do so, we follow and refine the procedure detailed in [54] (note that similar eccentric expansion techniques were also described shortly prior in [56]). The process requires that $X_{lmn}^{\pm}$ be evaluated at the location of the particle as it follows a generic, bound geodesic on the Schwarzschild background. In order to maintain a consistent PN description of the system, we must PN expand this motion, something that can be done to arbitrary order.

The basic framework for Schwarzschild geodesic motion was described in Sec. II C. An alternative description of the geodesic orbit known as the Darwin parametrization is much more useful for PN expansions. The Darwin parametrization recasts $\mathcal{E}$ and $\mathcal{L}$ in terms of the geometric quantities $p$, the (dimensionless) semilatus rectum, and $e$, the eccentricity [124–126]. These are related by

$$\mathcal{E}^2 = \frac{(p-2)^2-4e^2}{p(p-3-e^2)}, \qquad \mathcal{L}^2 = \frac{p^2M^2}{p-3-e^2}. \quad (4.1)$$

Bound orbits now satisfy $p > 6+2e$, with the boundary $p = 6+2e$ representing the separatrix [125].

It is of note that $1/p$ is a 1PN quantity, meaning PN series can be equivalently constructed by expanding in terms of $1/p$. We will thus expand the coordinate position of the particle in $1/p$ and eventually use this to expand the homogeneous solutions (evaluated at $r_p$) in $1/p$ as well. This formulation is well suited for the expansions of the fluxes, and it will also be used in Sec. VI to derive the relationship between certain BHPT-PN expansions in Schwarzschild coordinates and more standard PN expansions in modified harmonic coordinates. For the fluxes series in $e$ will also be made at each order in $1/p$ to make the normalization constants integrable.

The Darwin parametrization also shifts the curve parameter from proper time $\tau$ to the relativistic anomaly $\chi$, putting the radial position into the form

$$r_p(\chi) = \frac{pM}{1+e\cos\chi}. \quad (4.2)$$

One radial libration makes a change $\Delta\chi = 2\pi$. The remaining coordinates can be found as functions of $\chi$ through a set of ordinary differential equations:

$$\frac{dt_p}{d\chi} = \frac{r_p(\chi)^2}{M(p-2-2e\cos\chi)}\left[\frac{(p-2)^2-4e^2}{p-6-2e\cos\chi}\right]^{1/2}, \qquad \frac{d\varphi_p}{d\chi} = \left[\frac{p}{p-6-2e\cos\chi}\right]^{1/2}. \quad (4.3)$$

There is an analytic solution for the azimuthal motion,

$$\varphi_p(\chi) = \left(\frac{4p}{p-6-2e}\right)^{1/2} F\left(\frac{\chi}{2}\middle| -\frac{4e}{p-6-2e}\right), \quad (4.4)$$

where $F(\varphi|m)$ is the incomplete elliptic integral of the first kind [127]. The time coordinate, meanwhile, is expanded in $1/p$ and $e$ before integrating. The series begins

$$t_p(\chi) = (\chi - 2\sin(\chi)e + \mathcal{O}(e^2))p^{3/2} + (3\chi - 3\sin(\chi)e + \mathcal{O}(e^2))p^{1/2} + \mathcal{O}(p^{-1/2}). \quad (4.5)$$

This integration also provides the radial period and frequency:

$$T_r = \int_0^{2\pi}\left(\frac{dt_p}{d\chi}\right)d\chi = t_p(2\pi) - t_p(0) = \frac{2\pi}{\Omega_r}. \quad (4.6)$$

The mean azimuthal frequency follows as

$$\Omega_\varphi = \frac{\varphi(2\pi)}{T_r} = \frac{4}{T_r}\left(\frac{p}{p-6-2e}\right)^{1/2} K\left(-\frac{4e}{p-6-2e}\right), \quad (4.7)$$

where $K(m)$ is the complete elliptic integral of the first kind [127]. Finally, the compactness parameter $y$, which is a common (gauge-invariant) post-Newtonian expansion variable, is given by $y = (M\Omega_\varphi)^{2/3}$. It is easy to transform any given PN expansion from $1/p$ to $y$ and vice versa. Therefore, we will work with expansions in $1/p$ until the very end. Expansions in $y$ for the source motion and normalization constants can be found in [54]. Note that the PN series for the coordinates can be trivially applied to expand the source terms (2.15) and (2.16).

### B. The $C_{lmn}^{\pm}$ integrals

The inhomogeneous solutions are found by integrating the source motion for the constants $C_{lmn}^{\pm}$. This is most conveniently achieved in terms of $\chi$, using

$$C^{\pm}_{lmn} = \frac{1}{W_{lmn} T_r} \int_0^{2\pi} \left(\frac{dt}{d\chi}\right) \left[\frac{1}{f_p} G_{lm}(\chi) X^{\mp}_{lmn} + \left(\frac{2M}{r_p^2 f_p^2} X^{\mp}_{lmn} - \frac{1}{f_p}\frac{dX^{\mp}_{lmn}}{dr}\right) F_{lm}(\chi)\right] e^{i\omega t(\chi)} d\chi. \quad (4.8)$$

The homogeneous solutions are expressed as functions of $\chi$ by setting

$$z_p = r_p \omega = \frac{pM\omega}{1 + e\cos(\chi)} = \frac{M\bar{\omega}}{p^{1/2}(1 + e\cos(\chi))},$$
$$\epsilon = 2M\omega = \frac{2M\bar{\omega}}{p^{3/2}}, \quad (4.9)$$

where we have introduced a PN-adjusted frequency $\bar{\omega} = \omega p^{3/2} = \mathcal{O}(1)$. As with $\bar{z}$ and $\bar{\epsilon}$ in Sec. III, the use of the Newtonian-order $\bar{\omega}$ implies that every quantity within the expansions for $X^{\pm}_{lmn}$ is Newtonian order except for the expansion variable, which in this case is $1/p$. Thus, the PN order will now be tracked with $1/p$ alone, and the previous expansion parameter $\eta = 1/c$ can be set to 1. All series are now crafted to use the variables $1/p$ and $e$. This also allows us to avoid evaluating $\bar{\omega}$ in terms of $\Omega_r$ and $\Omega_\varphi$ until the end, which saves computational time.

The last needed quantity is the Wronskian $W_{lmn}$, given by

$$W_{lmn} = f \frac{dX^{+}_{lmn}}{dr} X^{-}_{lmn} - f \frac{dX^{-}_{lmn}}{dr} X^{+}_{lmn}. \quad (4.10)$$

Interestingly, this quantity is parity-independent. This can be shown by direct evaluation using the Detweiler-Chandrasekar transformation, along with the RW equation and $z$ independence of the result.

Overall, these integrals constitute the computational bottleneck in this analytic expansion procedure. When reduced entirely to series in $1/p$ and $e$, the result is a large sum of complex exponentials, which are trivial to integrate but extremely time consuming to handle. However, the simplifications detailed above serve to reduce the size of the expanded integrand by multiple orders of magnitude. This allows the procedure above to reach incredibly high PN orders in manageable time. A representative sample of benchmarks is given in Table III.

As an example, the expansion for the even-parity $2m1$ mode begins

$$C^{+}_{2m1} = \left[\left(\frac{16\bar{\omega}^2}{15} - \frac{8\bar{\omega}^3}{15}\right)e + \mathcal{O}(e^2)\right]\frac{1}{p} + \left[\left(-\frac{20\bar{\omega}^2}{9} - \frac{8m\bar{\omega}^2}{45} - \frac{4m^2\bar{\omega}^2}{45} + \frac{4m^2\bar{\omega}^3}{45} - \frac{16\bar{\omega}^4}{105} + \frac{16\bar{\omega}^5}{315}\right)e + \mathcal{O}(e^2)\right]\frac{1}{p^2} + \left[\left(-\frac{136i\bar{\omega}^3}{45} + \frac{68i\bar{\omega}^4}{45}\right)e + \mathcal{O}(e^2)\right]\frac{1}{p^{5/2}} + \mathcal{O}\left(\frac{1}{p^{7/2}}\right). \quad (4.11)$$

### C. Construction of the fluxes from the factored normalization constants

With the (factored) constants $C^{\pm}_{lmn}$ analytically expanded, we can pursue the fluxes with the formulas given in Sec. II D:

$$\left\langle \frac{dE}{dt} \right\rangle^{\infty} \Rightarrow \frac{1}{64\pi} \sum_{lmn} (l+2)(l+1)(l)(l-1)\omega^2 |C^{+}_{lmn}|^2,$$
$$\left\langle \frac{dL}{dt} \right\rangle^{\infty} \Rightarrow \frac{1}{64\pi} \sum_{lmn} (l+2)(l+1)(l)(l-1)m\omega |C^{+}_{lmn}|^2. \quad (4.12)$$

However, the flux expressions are still missing the $z$-independent factors that were removed in Sec. III E. These must be multiplied back in to retrieve the fluxes.

At infinity, the necessary term comes from the $z$-independent factors removed from $X^{+}_{lmn}$, as this function only appears in the Wronskian. On the other hand, the $z$-independent factors for $X^{-}_{lmn}$ in $1/W_{lmn}$ will cancel with similar factors in the normalization integral, so those can be ignored. We get

$$C^{+}_{\rm flux} = (-2i\epsilon)^{i\epsilon}(-i\epsilon p)^{\Delta\nu}\left(\frac{\Gamma(1+\Delta\nu-i\epsilon)}{\Gamma(1+2\Delta\nu)}\right) C^{+}_{\rm fac}, \quad (4.13)$$

where $C^{+}_{\rm fac}$ is the factorized normalization constant, while $C^{+}_{\rm flux}$ is the full constant utilized in the flux formulas. Then, the fluxes are found from

$$|C^{+}_{\rm flux}|^2 = e^{\pi\epsilon}(\epsilon p)^{2\Delta\nu} \frac{|\Gamma(1+\Delta\nu-i\epsilon)|^2}{\Gamma(1+2\Delta\nu)^2} |C^{+}_{\rm fac}|^2. \quad (4.14)$$

Note that this is identical to Johnson-McDaniel's $S_{lmn}$ factorization [72,90]. Similar factors appear in the fluxes at the larger black hole's horizon. These will be described in a future paper [128].

The flux modes have different starting orders in $1/p$ and $e$. Specifically, mode $lmn$ will begin at relative PN order $l-1$ in the odd-parity sector and $l-2$ in the even parity sector. The eccentricity series will begin at $e^{2|n|}$ in either case. Therefore, once target orders are established, the exact (finite) number of required modes can be determined. Computations can be separately made and stored for specific modes, which is a fast process on supercomputing clusters. In practice, this generally works by making two full computations for each value of $l$ (one for each parity) while leaving $m$ and $n$ general until the end. Then, the resulting contributions can be summed over $l$, $m$, and $n$ in a straightforward fashion.

## V. THE ENERGY AND ANGULAR MOMENTUM FLUX EXPANSIONS

### A. Form of the expansions and past work

When the expansions are completed, we find that the energy flux at infinity for eccentric-orbit Schwarzschild EMRIs can be written in the following form [20,43,44]:

$$\left\langle \frac{dE}{dt} \right\rangle^{\infty} = \frac{32}{5}\left(\frac{\mu}{M}\right)^2 y^5[\mathcal{L}_0 + y\mathcal{L}_1 + y^{3/2}\mathcal{L}_{3/2} + y^2\mathcal{L}_2 + y^{5/2}\mathcal{L}_{5/2} + y^3(\mathcal{L}_3 + \log(y)\mathcal{L}_{3L}) + \mathcal{L}_{7/2}y^{7/2} + y^4(\mathcal{L}_4 + \log(y)\mathcal{L}_{4L}) + y^{9/2}(\mathcal{L}_{9/2} + \log(y)\mathcal{L}_{9/2L}) + y^5(\mathcal{L}_5 + \log(y)\mathcal{L}_{5L}) + y^{11/2}(\mathcal{L}_{11/2} + \log(y)\mathcal{L}_{11/2L}) + y^6(\mathcal{L}_6 + \log(y)\mathcal{L}_{6L} + \log^2(y)\mathcal{L}_{6L2}) + y^{13/2}(\mathcal{L}_{13/2} + \log(y)\mathcal{L}_{13/2L}) + \cdots], \tag{5.1}$$

where each PN term $\mathcal{L}_i = \mathcal{L}_i(e)$ is a general function of $e$. The angular momentum flux has a nearly identical form [87]:

$$\left\langle \frac{dL}{dt} \right\rangle^{\infty} = \frac{32}{5}\left(\frac{\mu^2}{M}\right) y^{7/2}[\mathcal{J}_0 + y\mathcal{J}_1 + y^{3/2}\mathcal{J}_{3/2} + y^2\mathcal{J}_2 + y^{5/2}\mathcal{J}_{5/2} + y^3(\mathcal{J}_3 + \log(y)\mathcal{J}_{3L}) + \mathcal{J}_{7/2}y^{7/2} + y^4(\mathcal{J}_4 + \log(y)\mathcal{J}_{4L}) + y^{9/2}(\mathcal{J}_{9/2} + \log(y)\mathcal{J}_{9/2L}) + y^5(\mathcal{J}_5 + \log(y)\mathcal{J}_{5L}) + y^{11/2}(\mathcal{J}_{11/2} + \log(y)\mathcal{J}_{11/2L}) + y^6(\mathcal{J}_6 + \log(y)\mathcal{J}_{6L} + \log^2(y)\mathcal{J}_{6L2}) + y^{13/2}(\mathcal{J}_{13/2} + \log(y)\mathcal{J}_{13/2L}) + \cdots]. \tag{5.2}$$

The $\mathcal{J}$ functions are similar in structure to their $\mathcal{L}$ counterparts, and all computations in this paper were made equally for both; therefore, from this point we primarily discuss the energy case but emphasize that the angular momentum is exactly analogous.

It is important to note that because the techniques described in Secs. III and IV require expansion in $e$ at each PN order, each $\mathcal{L}_i(e)$ will be computed as a Taylor series about $e = 0$. However, in principle these flux terms can often be written as more compact functions of $e$. Indeed, the full PN theory using the multipolar post-Minkowskian (MPM) PN formalism yields PN terms as simpler expressions involving source multipole moments [20]. These can usually be evaluated to obtain any given PN term either as a (closed-form) rational function or as a compact Fourier summation that can be expanded to high order in $e$ [72,73,94]. For example, $\mathcal{L}_0$ and $\mathcal{L}_1$ can be found via PN theory to be [53,129,130]

$$\mathcal{L}_0 = \frac{1}{(1-e^2)^{7/2}}\left(1 + \frac{73}{24}e^2 + \frac{37}{96}e^4\right), \tag{5.3}$$

$$\mathcal{L}_1 = \frac{1}{(1-e^2)^{9/2}}\left(-\frac{1247}{336} - \frac{15901}{672}e^2 - \frac{9253}{384}e^4 - \frac{4037}{1792}e^6\right). \tag{5.4}$$

Interestingly, these closed forms for $\mathcal{L}_0$ and $\mathcal{L}_1$ can be extracted from their corresponding Taylor series simply by pulling out the initial eccentricity singular factors. Eccentric singularities such as these occur in all PN terms, though most do not reveal rational functions such as $\mathcal{L}_0$ and $\mathcal{L}_1$ (see [53,72,87] for more details). As a result, once the series in $e$ are found for each $\mathcal{L}_i$ using BHPT, we use knowledge from PN theory to resum the expansions in $e$ to improve convergence and, when possible, extract closed forms that would otherwise be much more difficult to derive through PN theory alone [72,73].

The expansions computed in this paper extend a recent sequence of advances on the eccentric-orbit fluxes. In 2009 Arun *et al.* completed derivation of the energy and angular momentum fluxes to 3PN for arbitrary-mass-ratio binaries [94,95,131], continuing the work of [129,130,132–135]. Those efforts revealed that $\mathcal{L}_0, \mathcal{L}_1, \mathcal{L}_2, \mathcal{L}_{3L}$ all have closed forms. The remaining terms $\mathcal{L}_{3/2}, \mathcal{L}_{5/2}, \mathcal{L}_3$ do not, but the use of computational techniques laid out in [53,72,73,87,94] permits their expansion to arbitrary order in $e$. The angular momentum case is identical in form.

Beyond 3PN order, explicit eccentricity expansions have primarily been calculated using BHPT. This was first pursued in 2016 in [53,136], which extracted coefficients in the flux expansions using a numeric-analytic fitting procedure. Broadly speaking this worked as follows: First, full numeric BHPT fluxes were computed for a two-dimensional grid of orbits covering roughly 50 choices of $p$ and 35 choices of $e$ (∼1750 total orbits). Then, these numeric results were fit to the double series. By computing this fit to high precision (hundreds of significant digits), the authors were able in certain cases to determine analytic forms for the coefficients by applying the integer relation algorithm PSLQ [88]. The result was the extraction of varying numbers of new eccentricity coefficients in the two fluxes through 7PN.

More recently, the authors of [87] repeated and improved this endeavor by instead fitting the individual *lmn* modes of the fluxes. These modes are characterized by certain

structures that simplify the fitting process and greatly increase the output. This permitted the extraction of many more eccentricity coefficients from 3.5PN to 9PN in both the energy and angular momentum regimes. See [87] for additional details.

Finally, work in [72,73] used complementary discoveries from BHPT and PN theory to find convenient forms for certain infinite sets of logarithmic terms in the fluxes. In particular, closed-form eccentricity series were discovered for all flux terms of the form $\mathcal{L}_{(3k)L(k)}$ and $\mathcal{L}_{(3k+1)L(k)}$ for integers $k \geq 0$. Simultaneously, methods were derived to determine to arbitrary order in $e$ all flux terms of the form $\mathcal{L}_{(3k+3/2)L(k)}$, $\mathcal{L}_{(3k+5/2)L(k)}$, $\mathcal{L}_{(3k+3)L(k)}$, and $\mathcal{L}_{(3k+4)L(k)}$ for $k \geq 0$. From those, members of the first two sets can be computed to arbitrary order in $e$ immediately, while members of the second two sets require lengthy precomputations using BHPT. Additional simplifications were made in the sets $\mathcal{L}_{(3k+9/2)L(k)}$ and $\mathcal{L}_{(3k+11/2)L(k)}$. The sets $\mathcal{L}_{(3k)L(k)}$ and $\mathcal{L}_{(3k+3/2)L(k)}$ are collectively referred to as the leading logarithm series [72,137], and $\mathcal{L}_{(3k+1)L(k)}$ and $\mathcal{L}_{(3k+5/2)L(k)}$ as the 1PN logarithm series [73]. $\mathcal{L}_{(3k+3)L(k)}$ and $\mathcal{L}_{(3k+9/2)L(k)}$ form the subleading or 3PN logarithm series, while $\mathcal{L}_{(3k+4)L(k)}$ and $\mathcal{L}_{(3k+11/2)L(k)}$ form the 4PN logarithm series [72,73].

The various past results for eccentric-orbit EMRI flux expansions are summarized and compared to the present work in Table IV. Of course, essentially all the energy flux terms in both this and past work were derived with an angular momentum counterpart, usually to the exact same order in $e$.

### B. Analytic expansion results for the fluxes

With previous efforts as a guide, the analytic expansion methods above were used to compute the two fluxes to high PN order, extending the low-PN high-$e$ results of [72,73,87] to 19PN and $e^{10}$. Note that because the orders in $y$ and $e$ must be fixed at the beginning of the procedure, it is not possible to obtain any individual terms to higher PN order as was possible with fitting [87]. However, what can be done is the execution of the entire procedure multiple times in order to retrieve low-PN terms to higher order in $e$. Therefore, in addition to obtaining the fluxes to 19PN and $e^{10}$, we also calculated them to 10PN and $e^{20}$.

In total, all PN terms 10PN and below are now known to at least $e^{20}$, and all PN terms from 10.5PN to 20PN are known to at least $e^{10}$. However, for many flux terms, particularly at low PN, $e$ power series computed in previous works remain the state of the art. An optimal expansion can be formed by selecting the highest power of $e$ found at each order. This is summarized in Table IV.

It is interesting to evaluate the relative strengths of fitting and direct analytic expansions, two very different approaches to computing the BHPT-PN series. In particular, the fitting approach is particularly adept at reaching high orders in eccentricity but is computationally expensive and limited to fairly low PN order. In contrast, the direct analytic method has some trouble calculating arbitrary orders in $e$, but it is versatile and excellent at moving to high PN. Thus, in some sense the two methods are complementary. However, due to the known need for

TABLE IV. Overview of past and present work on EMRI flux expansions through 19PN. Terms from 0PN to 3PN were derived using the full PN theory. The rest were found by the authors of [53] ("FEH16"), [87] ("MEHF20"), [72] ("ME19"), [73] ("ME20"), and the present work. Boxes in the body of the table indicate the order in eccentricity extracted in the listed paper. Boxes labeled "CF" were found in closed form, while those labeled "AO" can be rapidly computed to arbitrary order. Those labeled "AO*" can be found to arbitrary order only after (yet to be completed) lengthy precomputations are made using BHPT. The columns labeled "Max" take the highest power of $e$ found among all given sources. A comparable chart can be constructed for the angular momentum flux.

| Term | FEH16 | MEHF20 | ME19 | ME20 | This | Max | Term | FEH16 | MEHF20 | ME19 | ME20 | This | Max |
|---|---|---|---|---|---|---|---|---|---|---|---|---|---|
| $\mathcal{L}_{7/2}$ | $e^{24}$ | $e^{30}$ | ⋯ | ⋯ | $e^{20}$ | $e^{30}$ | $\mathcal{L}_{7L2}$ | $e^{2}$ | CF | ⋯ | CF | CF | CF |
| $\mathcal{L}_{4}$ | $e^{6}$ | $e^{30}$ | ⋯ | AO | $e^{20}$ | AO | $\mathcal{L}_{15/2}$ | ⋯ | $e^{12}$ | ⋯ | ⋯ | $e^{20}$ | $e^{20}$ |
| $\mathcal{L}_{4L}$ | CF | CF | ⋯ | CF | CF | CF | $\mathcal{L}_{15/2L}$ | ⋯ | $e^{26}$ | ⋯ | ⋯ | $e^{20}$ | $e^{26}$ |
| $\mathcal{L}_{9/2}$ | $e^{2}$ | $e^{30}$ | ⋯ | ⋯ | $e^{20}$ | $e^{30}$ | $\mathcal{L}_{15/2L2}$ | ⋯ | $e^{28}$ | AO | ⋯ | $e^{20}$ | AO |
| $\mathcal{L}_{9/2L}$ | $e^{18}$ | $e^{30}$ | AO | ⋯ | $e^{20}$ | AO | $\mathcal{L}_{8}$ | ⋯ | $e^{0}$ | ⋯ | ⋯ | $e^{20}$ | $e^{20}$ |
| $\mathcal{L}_{5}$ | $e^{0}$ | $e^{30}$ | ⋯ | ⋯ | $e^{20}$ | $e^{30}$ | $\mathcal{L}_{8L}$ | ⋯ | $e^{18}$ | ⋯ | ⋯ | $e^{20}$ | $e^{20}$ |
| $\mathcal{L}_{5L}$ | $e^{24}$ | CF | ⋯ | ⋯ | $e^{20}$ | CF | $\mathcal{L}_{8L2}$ | ⋯ | CF | ⋯ | ⋯ | $e^{20}$ | CF |
| $\mathcal{L}_{11/2}$ | $e^{2}$ | $e^{30}$ | ⋯ | ⋯ | $e^{20}$ | $e^{30}$ | $\mathcal{L}_{17/2}$ | ⋯ | $e^{2}$ | ⋯ | ⋯ | $e^{20}$ | $e^{20}$ |
| $\mathcal{L}_{11/2L}$ | $e^{10}$ | $e^{30}$ | ⋯ | AO | $e^{20}$ | AO | $\mathcal{L}_{17/2L}$ | ⋯ | $e^{16}$ | ⋯ | ⋯ | $e^{20}$ | $e^{20}$ |
| $\mathcal{L}_{6}$ | $e^{0}$ | $e^{20}$ | ⋯ | ⋯ | $e^{20}$ | $e^{20}$ | $\mathcal{L}_{17/2L2}$ | ⋯ | $e^{20}$ | ⋯ | AO | $e^{20}$ | AO |
| $\mathcal{L}_{6L}$ | $e^{2}$ | $e^{30}$ | AO | ⋯ | $e^{20}$ | AO | $\mathcal{L}_{9}$ | ⋯ | ⋯ | ⋯ | ⋯ | $e^{20}$ | $e^{20}$ |
| $\mathcal{L}_{6L2}$ | $e^{12}$ | CF | CF | ⋯ | CF | CF | $\mathcal{L}_{9L}$ | ⋯ | ⋯ | ⋯ | ⋯ | $e^{20}$ | $e^{20}$ |
| $\mathcal{L}_{13/2}$ | $e^{0}$ | $e^{30}$ | ⋯ | ⋯ | $e^{20}$ | $e^{30}$ | $\mathcal{L}_{9L2}$ | ⋯ | ⋯ | AO* | ⋯ | $e^{20}$ | $e^{20}$ |
| $\mathcal{L}_{13/2L}$ | $e^{2}$ | $e^{30}$ | ⋯ | ⋯ | $e^{20}$ | $e^{30}$ | $\mathcal{L}_{9L3}$ | ⋯ | CF | CF | ⋯ | CF | CF |
| $\mathcal{L}_{7}$ | $e^{0}$ | $e^{12}$ | ⋯ | ⋯ | $e^{20}$ | $e^{20}$ | 9.5–10PN | ⋯ | ⋯ | ⋯ | ⋯ | $e^{20}$ | $e^{20}$ |
| $\mathcal{L}_{7L}$ | $e^{2}$ | $e^{26}$ | ⋯ | AO* | $e^{20}$ | $e^{26}$ | 10.5–19PN | ⋯ | ⋯ | ⋯ | ⋯ | $e^{10}$ | $e^{10}$ |

high-PN expressions, and the ability to still reach useful order in $e$, the analytic expansion techniques will likely be the preferred avenue in reproducing these results for other BHPT quantities (especially in the Kerr case), outside of a few niche scenarios.

Explicit terms in the fluxes at infinity, and illustrations of the structure contained therein, are discussed at length in [87]. Coefficients grow combinatorially in size with PN order, involving increasingly large combinations of transcendental numbers; therefore, we forego enumeration of higher-order analytic coefficients here. The full series are all provided at [91] as well as [92] for convenient retrieval. Instead, comparisons to numerical data are given below, allowing for assessment of the utility of these expansions.

### C. Comparison to numerical calculations and convergence of the eccentric expansion

#### 1. Mode flux comparisons

With the high-order expansions computed, it is beneficial to assess their utility by comparing to numerical calculations for several specific orbits. This is done in a few separate ways to evaluate the possibility of enhancing convergence using factorization techniques. Previous work on factorizations has primarily applied them on a mode-by-mode basis [59,71,90,115,117]. Therefore, we start by making comparisons for the individual 220 mode, proportional to $|C^{+}_{220}|^2$. Unfortunately, when working in this manner, low-order results and information from PN theory cannot be readily included. Therefore, we utilize composite expansions constructed by joining only the 10PN/$e^{20}$ and 19PN/$e^{10}$ results of this paper. We do this for the $1/p$ expansion natural to BHPT, as well as the more standard expansion in $y$.

We then apply to these composite series several factorization schemes to check for improved convergence. Specifically, we try a logarithmic resummation (also referred to as the exponential resummation), in which a new series is constructed from the logarithm of the flux, and then the numeric evaluation of the log series is exponentiated to obtain the result [90,138]. Similar procedures are executed with a reciprocal resummation (inspired by [59]) and a singular factor resummation, the latter resulting from the removal of the separatrix $1/(p-6-2e)$ in the $1/p$ fit. We also test the benefit of the $S_{lmn}$ factorization [see (4.14) and [90] ], both with and without the other resummations. Note that the application of the factorizations here result in the generation of new double expansions (in PN and $e$). In the case of the full flux analyzed below, resummations will only be applied at the PN level, with the eccentricity functions first evaluated numerically.

Comparisons are made for $p=\{10,20\}$, $e=\{1/10, 1/4, 1/2\}$, with the results summarized in Figs. 1 and 2. We find that the logarithmic and reciprocal factorization schemes begin to fail at relatively low $e$, implying that these approaches are likely not useful for eccentric binaries on an $lmn$ basis. Additionally, the $S_{lmn}$ factorization seems to have little effect in the majority of cases, with close overlap between the $S_{lmn}$ and standard varieties of the resummation schemes. However, it does provide a noticeable benefit for the orbit $p=20, e=1/2$.

It is noteworthy that the fit in $1/p$ seems consistently better than the fit in $y$. This is particularly true in the low-$p$, low-$e$ regime, where the removal of the separatrix produces the best match. Interestingly, though this separatrix ("ISO") factorization barely changes the series, it provides a clear benefit for $p=10$ and $e=\{1/10,1/4\}$, allowing for relative errors near $10^{-6}$. A few other methods not depicted were tried as well (e.g., the $\tilde{\tilde{S}}_{lmn}$ factorization [90]), but none provided additional improvement.

Unfortunately, it is clear for $p=10$ that the PN approximation for the 220 mode rapidly loses validity beyond $e=1/4$, as the best matching series at $e=1/2$ produced by the $S_{220}$ factorization still yields 1% error (with the rest much worse than that). Better resummations and higher-order series in $e$ will be required to produce faithful representations of the $lmn$ fluxes for $p\lesssim 10$ around this level. However, the fidelity is markedly improved further into the PN regime, as the smallest relative error achieved for $p=20$ and $e=1/2$ is still near $10^{-6}$, as seen in Fig. 2.

We can roughly assess how the radius of convergence of this double series changes with $e$ by evaluating each non-logarithmic PN coefficient numerically. This leaves a single expansion in $y$ (or $1/p$) with coefficients $\mathcal{L}^{220}_n(e)$ (or something similar for the $1/p$ expansion). The radius of convergence is given by $\lim_{n\to\infty}(\mathcal{L}^{220}_n(e))^{-1/n}$ [48]. For $e=0$, the high-order coefficients stabilize at a level that implies a minimal valid semilatus rectum around $3\lesssim p\lesssim 4$. We find this rises to $p\sim 5$ for $1/10\lesssim e\lesssim 1/4$, to $p\sim 6$ for $e=1/2$, and to $p\sim 10$ at $e=1$. Of course, these numbers are very approximate, as the high-order PN terms are only expanded to $e^{10}$. Nevertheless, a significant decrease in convergence with $e$ is apparent.

#### 2. Full flux comparisons

For the full flux, we make comparisons using a composite PN series formed from four sources: results from PN theory through 3PN (involving closed forms or high-order $e$ expansions), an expansion to $e^{30}$ at 3.5PN (from fitting), expansions to $e^{20}$ from 4PN–10PN, and expansions to $e^{10}$ from 10.5PN–20PN. We again construct two separate series in this fashion, one using $1/p$ as the PN variable and the other using $y$. At each PN order eccentricity factors of $(1-e^2)^k$ for some appropriate $k$ are isolated to enhance convergence.

We then apply to these composite series similar factorization methods to check for improvements in fidelity. This time, the factorizations are only applied at the PN

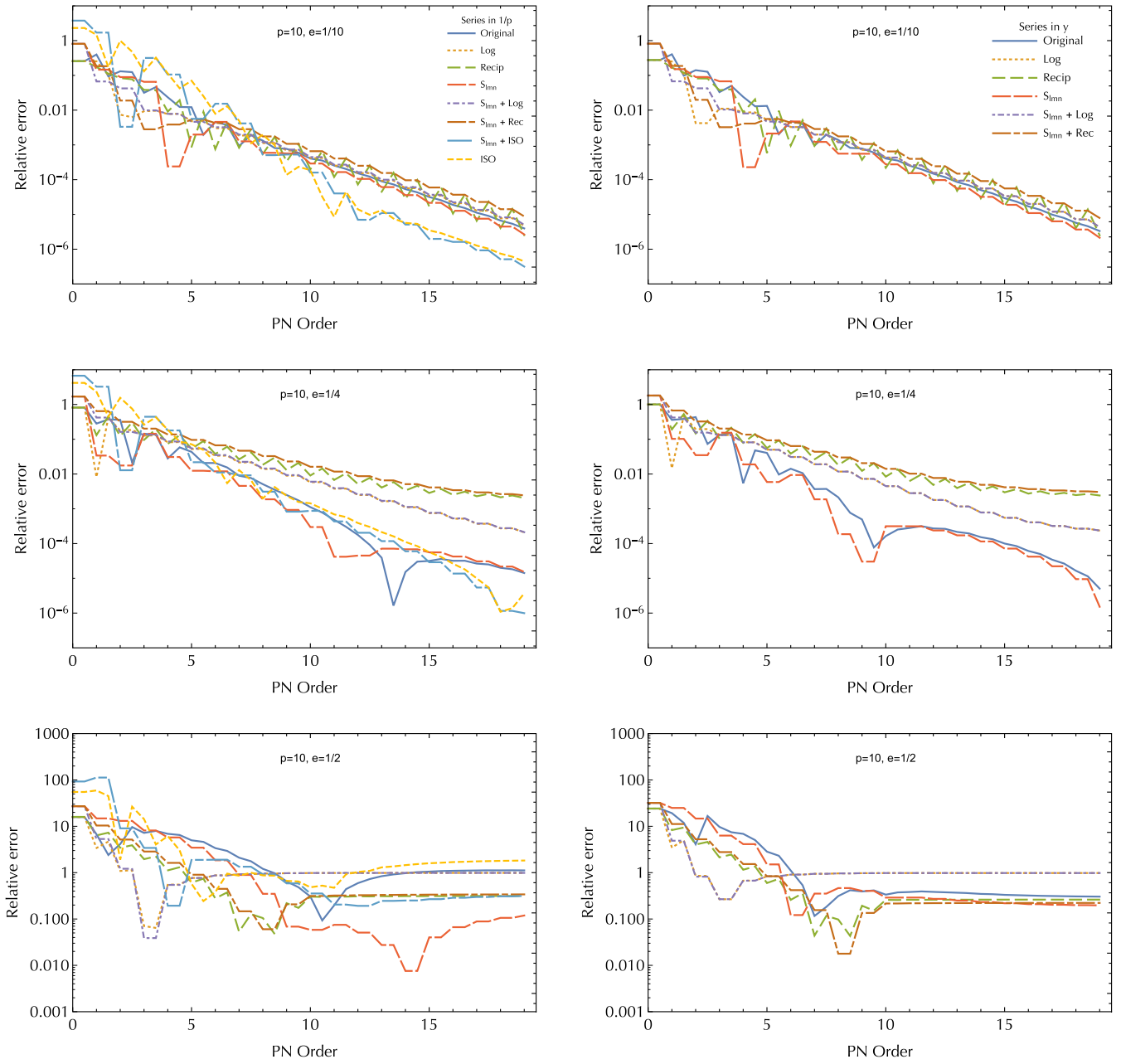


FIG. 1. Accuracy of the composite energy flux PN expansion and its resummations for the 220 mode for $p = 10$. The left column plots expansions in $1/p$ and $e$, while the right column plots their analogous expansions in $y$ and $e$. The $x$ axis denotes truncation of the series at the given PN order. Factorization schemes include logarithmic and reciprocal reexpansions, with and without removal of the $S_{220}$ factor. The $1/p$ expansion also includes reexpansion via the removal of the separatrix factor $1/(p-6-2e)$, labeled as "ISO" or "innermost stable orbit." Note the change in vertical scaling for $e = 1/2$.

expansion level, meaning that the eccentricity functions are evaluated numerically before the reexpansion is executed. This more easily preserves the closed forms and high-order expansions at low PN.

Comparisons are made for $p = 10$, $e = \{1/100, 1/10, 1/4, 1/2\}$, as depicted in Fig. 3. We find that the convergence is consistently better in the full-flux expansion than it was in the 220 mode, with the lowest error reaching $10^{-7}$ for $e = 1/4$ and $10^{-5}$ for $e = 1/2$. This is almost surely due to the use of closed forms and arbitrary-order expansions through 3PN, as well as the resummation of the eccentricity series at higher orders. It is noteworthy that the 4PN flux is already known to arbitrary order [73] while the 3.5PN flux is not, implying that a higher-order expansion for the latter would be desirable in moving further into the high-$e$, low-$p$ regime.

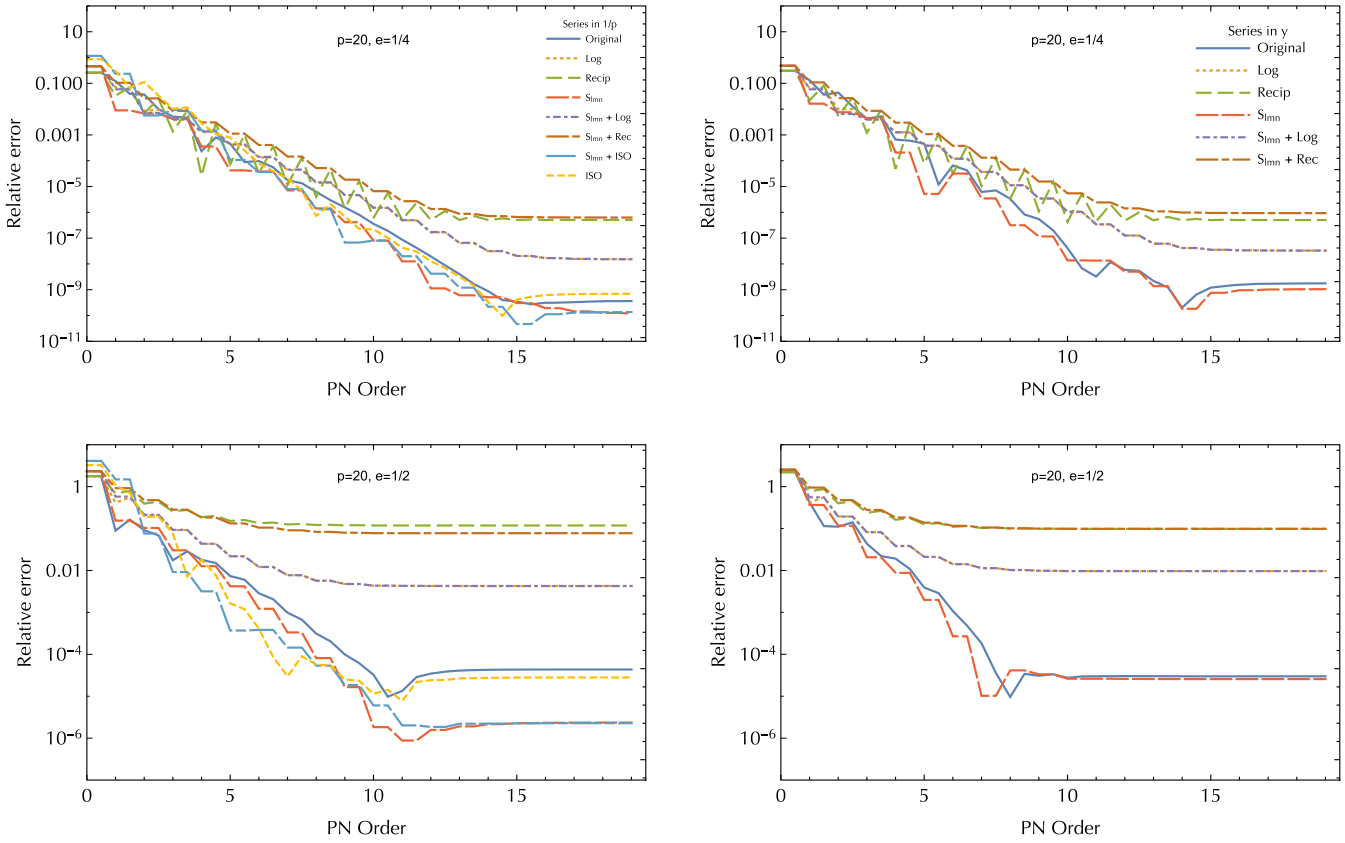


FIG. 2. Accuracy of the PN expansion and its resummations for the 220 mode for $p = 20$. The various labels and factorization schemes are identical to those in Fig. 1. Note the change in vertical scaling for $e = 1/2$.

There was not much consistency on the best expansion form across the four orbits. The $y$ expansions generally appear better than their $1/p$ counterparts at lower $e$, while the reverse seems to occur at higher $e$. The two factorizations do not affect the convergence of the $1/p$ expansions at low $e$, but both provide a clear benefit at $e = 1/4$ and $e = 1/2$. In contrast, the $y$ expansion resummations prove better than the original in all four cases, though the difference is fairly modest. From this small sample of orbits, we can potentially speculate that the reciprocal and logarithmic factorizations of the $y$ series provide the best match for small $e$, while the reciprocal resummation of the $1/p$ series may begin to outpace those as $e$ increases.

Despite the overall improved match over the 220 mode, the radius of convergence estimated through high-order coefficient magnitude appears worse in the full flux. The same procedure used in the mode flux reveals a minimally convergent $p \sim 4$ for $e = 0$. The eccentric cases yield $(e = 1/10, p \sim 5), (e = 1/4, p \sim 6), (e = 1/2, p \sim 8)$. Again, the low order of the eccentric expansions implies that these results are highly imprecise. However, this is sufficient to infer that the PN expansion loses strong-field validity in the high-eccentricity regime. Thus, it appears unlikely that BHPT-PN expansions can replace numeric calculations at the separatrix for highly eccentric fluxes. However, additional improvements are still possible through higher-order expansions. Note that even at $e = 1/2$, there is steady average improvement with increasing PN order in the full-flux expansion in Fig. 3. Thus, it will likely prove worthwhile to extend these series further and to continue to refine methods of factorization (perhaps by using Padé or Chebyshev approximants). Such explorations will be left to future work.

## VI. REPRESENTATION OF EMRI EXPANSIONS IN HARMONIC GAUGE

### A. Gauge dependence of the flux expansions and the quasi-Keplerian formalism

The previous sections detailed high-order PN series for the energy and angular momentum radiated to infinity by eccentric-orbit EMRIs. These expansions were derived from first-order BHPT using the RWZ formalism, which involves the use of Schwarzschild-RW coordinates. In particular, even though the fluxes themselves are gauge invariant, the quantities $p$ and $e$ are defined within the Darwin parametrization of Schwarzschild coordinates. Thus, the standard representation of BHPT flux expansions (and of all similar expansions) is dependent on those coordinates.

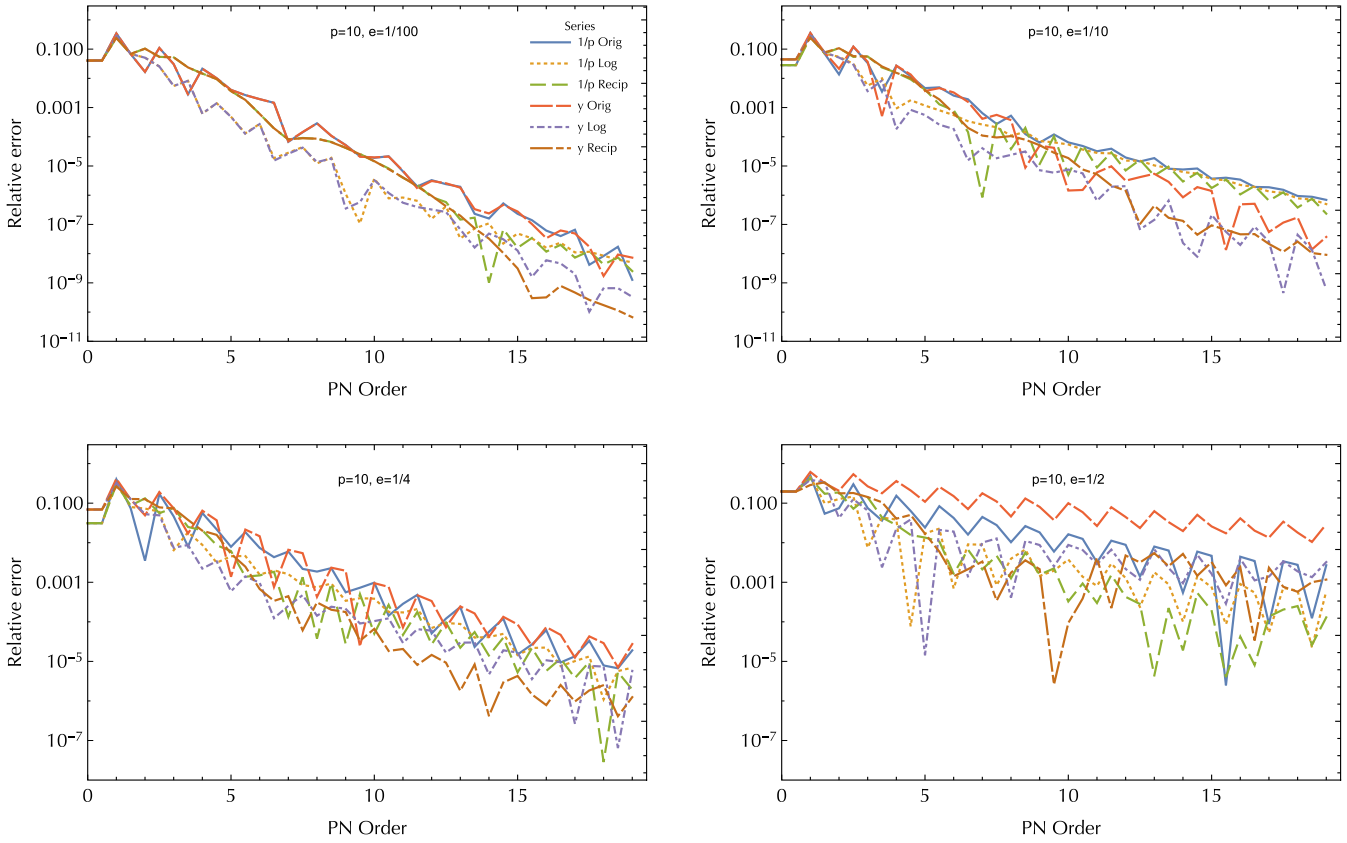


FIG. 3. Accuracy of the PN expansion and its resummations for the full flux for $p = 10$. Each plot corresponds to a different value of $e$. This time, in contrast to Figs. 1 and 2, the $1/p$ and $y$ expansions are superimposed on the same plots. Note the change in vertical scaling for the bottom two plots.

On the other hand, expansions found using the full PN theory are frequently derived in modified harmonic gauge, using QK parameters such as the so-called time eccentricity $e_t$, whose definition will be given below. It is possible to transform the fluxes from harmonic to Schwarzschild parameters by finding a PN expansion for $e_t$ in terms of $e$ (and vice versa). One way to relate $e_t$ to $e$ is to compute the expansion of each in terms of gauge-invariant quantities such as $\varepsilon$ and $j$ (related to the energy and angular momentum; see below) and then compare. In general, this can be done for $e_t$ only to the same PN order as the equations of motion, which have recently been completed to 4PN order [93], though the expansion for $e_t$ has only been published explicitly to 3PN [53,94–96].

However, BHPT presently offers the fluxes only at lowest order in the mass ratio. Thus, an expression for $e_t$ is similarly required only to lowest (zeroth) order in this mass ratio to enable transformation to and from harmonic gauge. This is possible through analysis of Schwarzschild geodesic motion. We show the procedure below and in the process derive the complete QK formalism for Schwarzschild geodesic motion to higher PN order.

We start by reviewing the current state of knowledge on the QK representation of nonspinning binary motion in general relativity. This description is modeled off the standard Keplerian equations of motion for elliptical orbits, given by

$$\begin{aligned} r &= a_r(1 - e_K \cos u), \\ \Omega_r t &= u - e_K \sin u, \\ \varphi &= V, \\ V &= 2 \arctan\left(\sqrt{\frac{1+e_K}{1-e_K}} \tan\frac{u}{2}\right). \end{aligned} \tag{6.1}$$

Here, $a_r$ is the semimajor axis, $e_K$ is the Keplerian eccentricity, $\Omega_r$ is the radial frequency, $u = u(t)$ is the eccentric anomaly, and $V$ is the true anomaly. At Newtonian order the motion is periodic, meaning $\Omega_r = \Omega_\varphi$ is the only frequency and the azimuthal coordinate $\varphi$ matches the true anomaly. $a_r$ and $e_K$ can be expressed in terms of other quantities as

$$\begin{aligned} a_r &= \frac{r_+ + r_-}{2} = \frac{M+\mu}{\varepsilon}, \\ e_K &= \frac{r_+ - r_-}{r_+ + r_-} = 1 - j. \end{aligned} \tag{6.2}$$

Here, we have defined $r_+ = r_{\max}, r_- = r_{\min}$ as the radii at apastron and periastron, respectively. Additionally,

$\varepsilon = -2E, j = -2EL^2/(M+\mu)^2$ are common parameters in PN work related to the energy and angular momentum of the system [20].

In 1985 Damour and Deruelle derived the 1PN relativistic corrections to these equations [139], leading to the following:

$$\begin{aligned} r_{\rm H} &= a_r(1 - e_r \cos u), \\ \Omega_r t &= u - e_t \sin u, \\ \varphi &= \left(\frac{\Omega_\varphi}{\Omega_r}\right) V = KV, \\ V &= 2\arctan\left(\sqrt{\frac{1+e_\varphi}{1-e_\varphi}}\tan\frac{u}{2}\right). \end{aligned} \tag{6.3}$$

Though similar in form, these relations present a few complications over the Keplerian motion. First, at 1PN order the motion no longer closes; thus, $\Omega_r \neq \Omega_\varphi$ and $\varphi \neq V$. Next, the single Keplerian eccentricity $e_K$ is supplanted by the threefold set of the radial eccentricity $e_r$, the time eccentricity $e_t$, and the azimuthal eccentricity $e_\varphi$, each of which has a different relationship to the energy and angular momentum of the system. Finally, the coordinates and parameters are all now defined in modified harmonic gauge [20]. The subscript on $r_{\rm H}$ has been added to emphasize that fact, distinguishing it from the Schwarzschild radius (however, the other coordinates do not require explicit labels for our purposes; see the next subsection).

Later work at 2PN [140,141] and then 3PN [96] implied a model for an effectively generic QK representation. This takes the form

$$\begin{aligned} r_{\rm H} &= a_r(1 - e_r \cos u), \\ \Omega_r t &= u - e_t \sin u + f_t \sin V + g_t(V-u) \\ &\quad + h_t \sin 2V + i_t \sin 3V + \cdots, \\ \frac{\varphi}{K} &= V + f_\varphi \sin 2V + g_\varphi \sin 3V + i_\varphi \sin 4V + \cdots, \\ V &= 2\arctan\left(\sqrt{\frac{1+e_\varphi}{1-e_\varphi}}\tan\frac{u}{2}\right). \end{aligned} \tag{6.4}$$

We have explicitly listed only those terms that appear in the 3PN QK equations but indicate that the series of trigonometric functions are expected to continue with higher PN orders.

Thus, the form of the radial motion is valid to all orders, with $e_r$ and $a_r$ defined by

$$e_r = \frac{r_{\rm H+} - r_{\rm H-}}{r_{\rm H+} + r_{\rm H-}}, \qquad a_r = \frac{r_{\rm H+} + r_{\rm H-}}{2}. \tag{6.5}$$

The $t$ and $\varphi$ equations, meanwhile, pick up trigonometric functions of $V$. In this generic representation, $e_\varphi$ is defined order by order to eliminate $\sin V$ from the equation for $\varphi$ [96]. The remaining parameters such as $e_t$ or $i_\varphi$ are defined simply as the coefficients in front of their respective trigonometric functions. Each is generally obtained as an expansion in $\varepsilon$ and $j$. As such, these parameters can, in principle, only be extracted to the same order as the full equations of motion, both of which come from iterating some formulation of the full PN formalism [20].

However, in the small-mass-ratio limit, the situation reduces to geodesic motion of the smaller body on a Schwarzschild background. Then, all the dynamics of the system are encoded in the geodesic equations of motion. We can thus apply the above definitions in this limit to generate the QK representation to all PN orders at lowest order in the mass ratio.

### B. Harmonic coordinates, Schwarzschild coordinates, and the Darwin parametrization

We now extract the QK description by looking at geodesic motion on a Schwarzschild background. First, the Schwarzschild metric can be expressed in the harmonic gauge as [142]

$$\begin{aligned} ds^2 = &-\frac{1 - M/r_{\rm H}}{1 + M/r_{\rm H}} dt_H^2 + \frac{1 + M/r_{\rm H}}{1 - M/r_{\rm H}} dr_{\rm H}^2 \\ &+ (r_{\rm H} + M)^2 d\Omega^2. \end{aligned} \tag{6.6}$$

In fact, these coordinates are almost identical to the standard Schwarzschild coordinates $(t_S, r_S, \theta_S, \varphi_S)$ with line element (2.1). The two are connected by

$$\begin{aligned} t_{\rm H} &= t_{\rm S} = t, \\ r_{\rm H} &= r_{\rm S} - M = r - M, \\ \theta_{\rm H} &= \theta_{\rm S} = \theta, \\ \varphi_{\rm H} &= \varphi_{\rm S} = \varphi. \end{aligned} \tag{6.7}$$

Therefore, we can work directly with the motion in Schwarzschild coordinates and merely correct the radius when necessary.

As described in Sec. IV A, geodesic motion in Schwarzschild coordinates is conveniently described using the Darwin parametrization, which for bound orbits recasts the specific energy $\mathcal{E} = (1 - \varepsilon/2)$ and angular momentum $\mathcal{L} = \sqrt{jM^2/\varepsilon}$ in terms of semilatus rectum $p$ and Darwin eccentricity $e$ [124–126]. $p$ and $e$ are defined by

$$p = \frac{2r_+ r_-}{M(r_+ + r_-)}, \qquad e = \frac{r_+ - r_-}{r_+ + r_-}, \tag{6.8}$$

with

$$r_+ = \frac{pM}{1-e},$$
$$r_- = \frac{pM}{1+e},$$
$$a = \frac{r_+ + r_-}{2} = \frac{pM}{1-e^2}. \tag{6.9}$$

Note that with the expressions (4.1) relating $\mathcal{E}$ and $\mathcal{L}$ to $p$ and $e$, $\varepsilon$ and $j$ can be immediately expanded to arbitrary order in $1/p$ and $e$, and these can be inverted to give $p$ and $e$ in terms of $\varepsilon$ and $j$. The result to 6PN is given in Appendix B.

Next, recall the QK definitions of $e_r$ and $a_r$ (6.5). Expressing these in terms of the Schwarzschild radius gives

$$e_r = \frac{r_+ - r_-}{r_+ + r_- - 2M},$$
$$a_r = \frac{r_+ + r_-}{2} - M. \tag{6.10}$$

Then, these can be related to $e$ and $p$ simply by

$$a_r = a - M = \frac{pM}{1-e^2} - M,$$
$$e_r = \frac{a}{a-M}e = \frac{p}{p-1+e^2}e. \tag{6.11}$$

This allows for the rapid expansion of $e_r$ and $a_r$ to arbitrary order in $p$ and $e$ and thus $\varepsilon$ and $j$. The two series are given to 6PN in Appendix B. Note that (6.11) immediately allows for the transformation of our BHPT-PN flux expansions to harmonic gauge to arbitrary PN order, except using $e_r$ instead of the more common $e_t$.

### C. Orbit integration and Kepler's equation

Further progress requires integration of the orbit. As mentioned in Sec. IV A this is described in terms of the relativistic anomaly $\chi$, reducing the coordinates to

$$r(\chi) = \frac{pM}{1+e\cos\chi},$$
$$\frac{dt}{d\chi} = \frac{p^2 M}{(p-2-2e\cos(\chi))(1+e\cos(\chi))^2} \times \left(\frac{(p-2)^2-4e^2}{p-6-2e\cos(\chi)}\right)^{1/2},$$
$$\varphi(\chi) = \left(\frac{4p}{p-6-2e}\right)^{1/2} F\left(\frac{\chi}{2}\middle| -\frac{4e}{p-6-2e}\right). \tag{6.12}$$

Given the form of these equations, a reasonable general definition for an eccentric anomaly, call it $\tilde{u}$, could be constructed analogously to its Newtonian counterpart, with

$$\chi = 2\arctan\left(\sqrt{\frac{1+e}{1-e}}\tan\frac{\tilde{u}}{2}\right). \tag{6.13}$$

From this definition, it can be found that

$$r = \left(\frac{pM}{1-e^2}\right)(1-e\cos\tilde{u}) = a(1-e\cos\tilde{u}). \tag{6.14}$$

But the corresponding QK equation is given by

$$r - M = r_{\rm H} = a_r(1-e_r\cos u)$$
$$= (a-M)\left(1-\frac{a}{a-M}e\cos u\right)$$
$$= a(1-e\cos u) - M. \tag{6.15}$$

Therefore, we observe that $u = \tilde{u}$ at lowest order in the mass ratio.

The relation between $\chi$ and $u$ can then be used to find

$$\frac{d\chi}{du} = \frac{\sqrt{1-e^2}}{1-e\cos u},$$
$$\frac{dt}{du} = \frac{p^2(1-e\cos u)^{5/2}\sqrt{(p-2)^2-4e^2}}{(1-e^2)^{3/2}(p(1-e\cos u)-2+2e^2)\sqrt{p-6+2e^2-e(p-4)\cos u}}. \tag{6.16}$$

The right-hand side of this equation can be expanded in $1/p$ (but left exact in $e$) and integrated to give $t(u)$ as a PN series to arbitrary order. When done in this way, the series starts

$$t(u) = \frac{u-e\sin u}{(1-e^2)^{3/2}}p^{3/2} + \frac{3u}{\sqrt{1-e^2}}\sqrt{p} + \left[6u - 2e\sin u + \frac{15}{2}\sqrt{1-e^2}\chi\right]\left(\frac{1}{\sqrt{1-e^2}\sqrt{p}}\right)$$
$$+ \left[12(5-e^2)u - 16e\sin u + 75\sqrt{1-e^2}\chi + 35e\sqrt{1-e^2}\sin\chi\right]\left(\frac{1}{2\sqrt{1-e^2}p^{3/2}}\right) + \mathcal{O}\left(\frac{1}{p^{5/2}}\right), \tag{6.17}$$

where we used that $\sin\chi = (\sqrt{1-e^2}\sin u)/(1-e\cos u)$. Then, the PN generalization of Kepler's equation for Schwarzschild geodesic motion (in terms of $u$ and $\chi$) can be trivially recovered through multiplication by $\Omega_r$. After rearranging terms, this gives

$$\Omega_r t = u + 15(1-e^2)^{3/2}\left[\frac{1}{2p^2}+\frac{6+9e^2}{2p^3}\right](\chi-u) + \frac{35(1-e^2)^{3/2}}{2p^3}e\sin\chi - e\sin u\left[1-\frac{3(1-e^2)}{p} + \frac{(1-e^2)(10-18e^2-15\sqrt{1-e^2})}{2p^2} - \frac{(1-e^2)(38-60e^2+54e^4-(15-90e^2)\sqrt{1-e^2})}{2p^3}\right] + \mathcal{O}\left(\frac{1}{p^4}\right). \tag{6.18}$$

The expression behind $\sin u$ in (6.18) can be identified as an expansion for $e_t/e$ in terms of $p$ and $e$. Transforming to $\varepsilon$ and $j$ reveals that this matches the 3PN expression for $e_t$ in modified harmonic coordinates given in [95]. As with $e_r$ and $a_r$, $e_t$ can be found in this way to arbitrary PN order. However, the procedure here—with both the execution of the integral for $t(u)$ and the identification of the $\sin n\chi$ terms—is far more cumbersome. Here is the result to 5PN:

$$\frac{e_t}{e} = 1-\frac{3(1-e^2)}{p} + \left(10-18e^2-15\sqrt{1-e^2}\right)\left(\frac{1-e^2}{2p^2}\right) - \left(38-60e^2+54e^4-(15-90e^2)\sqrt{1-e^2}\right)\left(\frac{1-e^2}{2p^3}\right) + \left(4(309-1006e^2+765e^4-324e^6) - 3\sqrt{1-e^2}(698-535e^2+1080e^4)\right)\left(\frac{1-e^2}{16p^4}\right) - \left(4(299-2839e^2+6777e^4 - 4185e^6+972e^8) + 3\sqrt{1-e^2}(954+6731e^2-4050e^4+4320e^6)\right)\left(\frac{1-e^2}{16p^5}\right) + \mathcal{O}\left(\frac{1}{p^6}\right). \tag{6.19}$$

Unfortunately, the completion of this procedure to 19PN would likely be difficult, implying that $e_r$ might be the preferable choice of eccentricity when transforming high-order BHPT-PN series to harmonic gauge. We present the expansion for $e_t$ in $\varepsilon$ and $j$ in Appendix B.

The above results indicate that the coefficient of $(\chi-u)$ does not equal $g_t$, and the coefficient of $\sin\chi$ does not equal $f_t$. This stems from the fact that $\chi \neq V$, as evidenced by comparing (6.4) and (6.13).

### D. The azimuthal equation

We can now pursue the rest of the QK parametrization, starting with the relationship between $\chi$ and $V$. This can be obtained using another equation of motion,

$$\frac{\varphi}{K} = \chi + \tilde{a}_\varphi\sin\chi + \tilde{f}_\varphi\sin 2\chi + \tilde{g}_\varphi\sin 3\chi + \tilde{i}_\varphi\sin 4\chi + \cdots = V + f_\varphi\sin 2V + g_\varphi\sin 3V + i_\varphi\sin 4V + \cdots, \tag{6.20}$$

where all given quantities are PN expanded to any desired order. As mentioned above, we see that $V$ is defined order by order to eliminate the appearance of $\sin V$ in the representation for $\varphi$. The expansion for $\varphi/K$ in terms of $\chi$ is easily computed using the Darwin parametrization as

$$\frac{\varphi}{K} = \chi + \frac{e\sin\chi}{p} + \frac{3e(16\sin\chi + e\sin 2\chi)}{8p^2} + \frac{(27e(32+e^2)\sin\chi + 108e^2\sin 2\chi + 5e^3\sin 3\chi)}{24p^3} + \mathcal{O}\left(\frac{1}{p^4}\right). \tag{6.21}$$

The exact relationship between $\chi$ and $V$ is given by

$$\chi = 2\arctan\left(\sqrt{\frac{1+e}{1-e}}\tan\frac{u}{2}\right) = 2\arctan\left(\sqrt{\frac{(1+e)(1-e_\varphi)}{(1-e)(1+e_\varphi)}}\tan\frac{V}{2}\right). \tag{6.22}$$

In order to eliminate $\sin V$ from (6.20), $\chi(V)$ is inserted. Then, $\varphi(\chi(V))/K$ is expanded using an ansatz for the PN series of $e_\varphi$ in $1/p$. The coefficients in this series are then exactly determined by the condition that $\sin V$ disappears from the representation for $\varphi/K$.

In this way, we obtain

$$\frac{e_\varphi}{e} = 1+\frac{1-e^2}{p}+\frac{(1-e^2)(6-e^2)}{p^2}+\frac{(1-e^2)(36-11e^2+e^4)}{p^3}+\frac{(1-e^2)(216-90e^2+16e^4-e^6)}{p^4} + (1296-648e^2+170e^4-21e^6+e^8)\left(\frac{1-e^2}{p^5}\right) + (7776-4320e^2+1500e^4-275e^6+26e^8-e^{10})\left(\frac{1-e^2}{p^6}\right) + \mathcal{O}\left(\frac{1}{p^7}\right). \tag{6.23}$$

This method can be (fairly rapidly) extended to arbitrary order, and we cover the expansion in $\varepsilon$ and $j$ in Appendix B.

From here, the expansion for $\chi(V)$ can be substituted into (6.20) to retrieve $f_\varphi, g_\varphi, \ldots$, and it can also be put into Kepler's equation to compute $f_t, g_t, \ldots$. These are less useful than the eccentricities for the purposes of expansion transformations, but the full forms of these equations are given in Appendix A.

## VII. CONCLUSIONS AND OUTLOOK

This paper has described the high-order analytic expansion of the total energy and angular momentum radiated to infinity by eccentric-orbit EMRIs. By extending the methods of [44,50] to the eccentric regime, we have computed both fluxes to 10PN and $e^{20}$, as well as to 19PN and $e^{10}$, a significant advance over previous work with numeric-analytic fitting [53,87]. We thus conclude that the direct analytic expansion scheme is highly successful at reaching high PN order and moderate order in eccentricity for the energy and angular momentum fluxes at infinity.

The high-order expansions in this work allow for a representation of the fluxes that is valid for small $p$ and moderate $e$ or large $p$ and fairly large $e$. Unfortunately, it does appear to experience some trouble in the small-$p$ large-$e$ regime. This is likely due at least in part to insufficient $n$ mode representation in the PN expansions. Indeed, while the PN expansions only include $|n|$ up to half the maximum eccentricity order, the numerical $(p = 10, e = 1/2)$ flux, for instance, accurate to 12 digits required $n$ higher than 20 for certain $lm$ modes. Therefore, higher-order expansions in $e$ are likely necessary to ensure convergence at higher $e$. Insufficient representation of $l$ modes has also been noted as a limiting factor for small $p$ [44,82].

The bottleneck step in the procedure was the calculation of the even-parity normalization constant for $l = 2$. This calculation took about 7 days on a single core of the UNC cluster Longleaf, indicating that another PN term or another couple orders in $e^2$ could be obtained with a long runtime or faster core. Nevertheless, significantly higher orders are probably out of reach with the current implementation of the code. It is possible that additional simplifications are yet undiscovered in the construction of the homogeneous or inhomogeneous solutions, which would allow for another large increase in attainable order. A reformulation in another language like PYTHON or C++ could also feasibly be advantageous.

However, more promising is the prospect of finding superior resummation schemes that will greatly increase the convergence to numerical calculations. Unfortunately, it appears that some of the straightforward mode-based factorizations applied successfully in the circular-orbit case will not be quite as fruitful in the high-eccentricity regime. Future work experimenting with more complex and unconventional factorization schemes (e.g., Pade or Chebyshev approximants) will be warranted.

Still, it is encouraging that the accuracy of the full-flux expansion was fairly strong even for the orbit $(p = 10, e = 1/2)$, owing to the use of arbitrary-order eccentricity expansions at low PN and the use of eccentricity resummations throughout. Increased validity at higher eccentricity can likely be obtained by extending these expansions to higher order in $e$, which is particularly important at lower PN order. To that end, the techniques developed in [72,73] can (in principle) be extended to derive expansions for the 3.5PN, 4.5PN, and 5PN terms to arbitrary order in $e$, though with considerable difficulty (especially at 4.5PN). This is achieved through intricate but manageable manipulations involving Fourier decomposition of source multipole moments (see [72,73] for more details). Beyond 5PN, further progress is likely more accessible to the MST analytic expansion approach of this paper. For instance, it may be possible to obtain the 6PN and 7PN terms beyond $e^{30}$ using the methods of Secs. III and IV, but this is not certain. In addition, the $e^{20}$ calculation can potentially be extended to 11PN or 12PN. These ideas will be explored in future work.

In the meantime the methods developed in this paper can also be utilized to generate expansions for other BHPT quantities of interest. The first and most obvious is the radiation at the larger black hole's horizon, found using the coefficients $C^{-}_{lmn}$. We have already calculated these to 10PN and $e^{20}$ and 18PN and $e^{10}$ (relative to the leading horizon flux) using the techniques laid out above, and the results will be detailed in a follow-up paper [128].

Beyond that, direct analytic expansion techniques have also been successfully applied in the conservative sector of BHPT. Conservative quantities supply crucial terms in EOB potentials (see, e.g., [49,54,61,67,75,76,81,97,143,144]) and also contribute directly to the EMRI cumulative phase at post-1 adiabatic order [83]. For instance, the authors of [50] found the redshift invariant, spin-precession invariant, and tidal invariants to 21.5PN order for circular-orbit EMRIs on a Schwarzschild background. Published results in the eccentric case are much more modest: For instance, the state of the art for the redshift invariant is 4PN and $e^{20}$ and 9.5PN and $e^8$ [54,58,76], while the others are even less developed [61,64]. In general, expansions in the conservative sector are more complicated, as the leading PN order of individual modes does increase with $l$, meaning that expansions are required that remain general in $l$. Nevertheless, techniques have been developed to handle this complication [50,54,79,80], and we report that we have extended the present work to the conservative sector and found the redshift invariant to 8.5PN and $e^{20}$. This will be discussed in a follow-up paper [145].

With generic bound orbits on a Schwarzschild background analytically understood, it will be necessary to extend these methods to the more intricate (but more

astrophysically relevant) Kerr background. There, analytic expansions are possible using the Teukolsky formalism, which is similar to the RWZ formalism of this paper, though more expensive by multiple orders of magnitude. Past work has primarily focused on expanding the simpler case of circular equatorial orbits [55,82,121], though flux series for generic (eccentric, inclined) orbits have been found to 4PN and $e^6$ [52]. The simplifications developed in this paper, when properly adapted to the Kerr case, should allow for a significant improvement over the state of expansions for generic orbits.

Finally, this paper has also presented a means to derive a quasi-Keplerian representation of Schwarzschild geodesic motion to high PN order. This allows for the rapid transformation between certain high-order PN series generated by BHPT and those derived through the full PN formalism in (modified) harmonic coordinates. The QK results obtained in this manner provide a nice check on future developments in PN theory, as the small-mass-ratio limit of any new results should match the prescription laid out here.

It is of note that we sought the particular QK representation in harmonic coordinates, but this is not the only available choice. By extracting the geodesic limit of some other gauge, we could repeat the above procedure and ascertain the QK parameters in that gauge. As an example, the authors of [142,146] indicate that the Schwarzschild limit of ADM gauge is given by isotropic coordinates:

$$ds^2 = -\left(\frac{2r_{\rm I} - M}{2r_{\rm I} + M}\right)^2 dt^2 + \left(1 + \frac{M}{2r_{\rm I}}\right)^4 (dr_{\rm I}^2 + r_{\rm I}^2 d\Omega^2) \tag{7.1}$$

with $r_{\rm S} = r_{\rm I}(1 + M/(2r_{\rm I}))^2$. This choice is amenable to the same techniques, though the more complicated relationship between the two radii will make the process somewhat more cumbersome.

In addition, Schwarzschild geodesic motion corresponds to the zeroth-order BHPT calculation; however, the first-order problem has also been (effectively) solved. Thus, it is theoretically feasible to extend this procedure to first order in the mass ratio, obtaining all contributions at $\mathcal{O}(\nu)$ in the QK representation. Deriving these corrections would be orders of magnitude more difficult, as geodesic motion on the first-order (regularized) metric is complicated [147]. Furthermore, the process of gauge transformation from first-order RW (or radiation) to harmonic coordinates is far more intricate than that from the simple Schwarzschild coordinates of geodesic motion [10,148,149]. We will leave further exploration of this problem for future work.

## ACKNOWLEDGMENTS

The author thanks Charles R. Evans, Adrian Ottewill, Barry Wardell, Nathan Johnson-McDaniel, Niels Warburton, Seth Hopper, Chris Kavanagh, and Zachary Nasipak for many helpful discussions. The author also thanks Jezreel Castillo for providing the numeric value of the flux for $(p = 10, e = 1/2)$ and Thomas Osburn for supplying additional flux data. This work makes use of the Black Hole Perturbation Toolkit. This work was supported in part by NSF Grants No. PHY-1506182 and No. PHY-1806447, the Bahnson Fund at the University of North Carolina-Chapel Hill, and the North Carolina Space Grant.

## APPENDIX A: THE KEPLER AND AZIMUTHAL EQUATIONS TO 5PN

The methods above can be used to generate higher-order corrections to the full Kepler's equation. In terms of $p$ and $e$, we get

$$\begin{aligned}\Omega_r t = {} & u - e_t \sin u + 3(1-e^2)^{3/2}\left[\frac{5}{2p^2} + \frac{5(2+3e^2)}{2p^3} + \frac{738 + 145e^2 + 360e^4 - 300(1-e^2)^{3/2}}{16p^4}\right. \\ & \left. + \frac{3528 + 3512e^2 - 165e^4 + 1080e^6 - 600(1-e^2)^{3/2}(2+3e^2)}{16p^5}\right](V-u) + e(1-e^2)^{3/2}\left[\frac{10}{p^3} + \frac{5(29+24e^2)}{4p^4}\right. \\ & \left. + \frac{3(722 + 267e^2 + 240e^4 - 200(1-e^2)^{3/2})}{8p^5}\right]\sin V + e^2(1-e^2)^{3/2}\left[\frac{95}{32p^4} + \frac{434 + 285e^2}{32p^5}\right]\sin 2V \\ & + e^3(1-e^2)^{3/2}\left(\frac{9}{8p^5}\right)\sin 3V + \mathcal{O}\left(\frac{1}{p^6}\right),\end{aligned} \tag{A1}$$

where $e_t$ is given in (6.19).

Likewise, $\chi(V)$ is plugged into the azimuthal equation to obtain

$$\begin{aligned}\frac{\varphi}{K} = {} & V + \frac{e^2 \sin 2V}{8p^2} + \frac{3e^2 \sin 2V}{2p^3} + \frac{\frac{1}{16}e^2(216 + 5e^2)\sin 2V + \frac{3}{256}e^4 \sin 4V}{p^4} \\ & + \frac{\frac{3}{2}e^2(72 + 5e^2)\sin 2V + \frac{9}{32}e^4 \sin 4V}{p^5} + \mathcal{O}\left(\frac{1}{p^6}\right).\end{aligned} \tag{A2}$$

## APPENDIX B: ORBITAL PARAMETERS EXPANDED IN $\varepsilon$ AND $j$

We now present expansions for various QK quantities in terms of the gauge invariant quantities $\varepsilon$ and $j$. These are found by using the expansions for $p$ and $e$, given to 6PN by

$$\begin{aligned}
p &= \frac{j}{\varepsilon} + (-4+j) + \left(4 - \frac{16}{j} + \frac{3j}{4}\right)\varepsilon + \left(3 - \frac{128}{j^2} + \frac{48}{j} + \frac{j}{2}\right)\varepsilon^2 + \left(2 - \frac{1280}{j^3} + \frac{640}{j^2} - \frac{12}{j} + \frac{5j}{16}\right)\varepsilon^3 \\
&\quad + \left(\frac{5}{4} - \frac{14336}{j^4} + \frac{8960}{j^3} - \frac{800}{j^2} + \frac{3j}{16}\right)\varepsilon^4 + \left(\frac{3}{4} - \frac{172032}{j^5} + \frac{129024}{j^4} - \frac{20160}{j^3} + \frac{320}{j^2} + \frac{7j}{64}\right)\varepsilon^5 + \mathcal{O}(\varepsilon^6), \\
e^2 &= (1-j) + \left(4 - \frac{7j}{4}\right)\varepsilon - \left(5 - \frac{16}{j} + 2j\right)\varepsilon^2 - \left(10 - \frac{128}{j^2} + \frac{52}{j} + \frac{15j}{8}\right)\varepsilon^3 - \left(\frac{45}{4} - \frac{1280}{j^3} + \frac{672}{j^2} + \frac{40}{j} + \frac{25j}{16}\right)\varepsilon^4 \\
&\quad - \left(\frac{41}{4} - \frac{14336}{j^4} + \frac{9280}{j^3} - \frac{320}{j^2} + \frac{35}{j} + \frac{77j}{64}\right)\varepsilon^5 - \left(\frac{133}{16} - \frac{172032}{j^5} + \frac{132608}{j^4} - \frac{15232}{j^3} + \frac{40}{j^2} + \frac{28}{j} + \frac{7j}{8}\right)\varepsilon^6 + \mathcal{O}(\varepsilon^7).
\end{aligned} \tag{B1}$$

First, the harmonic semimajor axis, $a_r = pM/(1-e^2) - M$, takes the form

$$\begin{aligned}
\frac{a_r}{M} &= \frac{1}{\varepsilon} - \frac{7}{4} + \left(\frac{1}{16} - \frac{4}{j}\right)\varepsilon + \left(\frac{1}{64} - \frac{32}{j^2} + \frac{4}{j}\right)\varepsilon^2 + \left(\frac{1}{256} - \frac{320}{j^3} + \frac{80}{j^2} - \frac{1}{j}\right)\varepsilon^3 \\
&\quad + \left(\frac{1}{1024} - \frac{3584}{j^4} + \frac{1344}{j^3} - \frac{68}{j^2}\right)\varepsilon^4 + \left(\frac{1}{4096} - \frac{43008}{j^5} + \frac{21504}{j^4} - \frac{2128}{j^3} + \frac{24}{j^2}\right)\varepsilon^5 + \mathcal{O}(\varepsilon^6).
\end{aligned} \tag{B2}$$

Next, the three eccentricities, $e_r^2 = (a/a_r)^2 e^2$, is given by

$$\begin{aligned}
e_r^2 &= 1 - j + \left(6 - \frac{15j}{4}\right)\varepsilon + \left(\frac{15}{2} + \frac{16}{j} - 10j\right)\varepsilon^2 - \left(\frac{1}{2} - \frac{128}{j^2} + \frac{12}{j} + \frac{93j}{4}\right)\varepsilon^3 \\
&\quad - \left(\frac{615}{16} - \frac{1280}{j^3} + \frac{352}{j^2} + \frac{76}{j} + \frac{201j}{4}\right)\varepsilon^4 + \left(-\frac{621}{4} + \frac{14336}{j^4} - \frac{6080}{j^3} - \frac{544}{j^2} - \frac{633}{2j} - \frac{1661j}{16}\right)\varepsilon^5 \\
&\quad + \left(-\frac{7385}{16} + \frac{172032}{j^5} - \frac{96768}{j^4} + \frac{576}{j^3} - \frac{2196}{j^2} - \frac{1047}{j} - 208j\right)\varepsilon^6 + \mathcal{O}(\varepsilon^7).
\end{aligned} \tag{B3}$$

The azimuthal eccentricity is similarly simple, giving

$$\begin{aligned}
e_\varphi^2 &= 1 - j + \left(6 - \frac{15j}{4}\right)\varepsilon + \left(-\frac{5}{2} + \frac{26}{j} - 10j\right)\varepsilon^2 + \left(-\frac{87}{2} + \frac{220}{j^2} - \frac{77}{2j} - \frac{93j}{4}\right)\varepsilon^3 \\
&\quad + \left(-\frac{2737}{16} + \frac{2298}{j^3} - \frac{646}{j^2} - \frac{313}{j} - \frac{201j}{4}\right)\varepsilon^4 + \left(-\frac{2033}{4} + \frac{26676}{j^4} - \frac{20981}{2j^3} - \frac{5021}{2j^2} - \frac{5373}{4j} - \frac{1661j}{16}\right)\varepsilon^5 \\
&\quad + \left(-\frac{21181}{16} + \frac{330020}{j^5} - \frac{167759}{j^4} - \frac{16342}{j^3} - \frac{177879}{16j^2} - \frac{72027}{16j} - 208j\right)\varepsilon^6 + \mathcal{O}(\varepsilon^7).
\end{aligned} \tag{B4}$$

The time eccentricity is more complicated, containing half powers of $j$, and is also more tedious to construct. We give it to 5PN:

$$\begin{aligned}
e_t^2 &= 1 - j - \left(2 - \frac{17j}{4}\right)\varepsilon + \left(\frac{3}{2} + \frac{8}{j} - \frac{15}{\sqrt{j}} + 15\sqrt{j} - 14j\right)\varepsilon^2 + \left(\frac{7}{2} + \frac{64}{j^2} - \frac{105}{j^{3/2}} - \frac{66}{j} + \frac{1365}{8\sqrt{j}} - \frac{795\sqrt{j}}{8} + \frac{165j}{4}\right)\varepsilon^3 \\
&\quad + \left(-\frac{3067}{16} + \frac{640}{j^3} - \frac{9009}{8j^{5/2}} - \frac{672}{j^2} + \frac{12879}{8j^{3/2}} + \frac{1795}{4j} - \frac{129645}{128\sqrt{j}} + \frac{56385\sqrt{j}}{128} - \frac{457j}{4}\right)\varepsilon^4 + \left(\frac{3207}{2} + \frac{7168}{j^4} - \frac{109395}{8j^{7/2}}\right. \\
&\quad \left. - \frac{8096}{j^3} + \frac{1291491}{64j^{5/2}} + \frac{11461}{2j^2} - \frac{1464531}{128j^{3/2}} - \frac{70841}{16j} + \frac{4517145}{1024\sqrt{j}} - \frac{1668795\sqrt{j}}{1024} + \frac{4867j}{16}\right)\varepsilon^5 + \mathcal{O}(\varepsilon^6).
\end{aligned} \tag{B5}$$

Note that these expansions match the expressions in [95] to 3PN at lowest order in $\nu$.

[1] L. Barack, V. Cardoso, S. Nissanke, T. P. Sotiriou *et al.*, Classical Quantum Gravity **36**, 143001 (2019).
[2] P. Amaro-Seoane, J. R. Gair, M. Freitag, M. C. Miller, I. Mandel, C. J. Cutler, and S. Babak, Classical Quantum Gravity **24**, R113 (2007).
[3] C. Berry, S. Hughes, C. Sopuerta, A. Chua, A. Heffernan, K. Holley-Bockelmann, D. Mihaylov, C. Miller, and A. Sesana, Bull. Am. Astron. Soc. **51**, 42 (2019); arXiv:1903.03686.
[4] LISA home page, http://sci.esa.int/lisa/.
[5] L. Barack and A. Pound, Rep. Prog. Phys. **82**, 016904 (2018).
[6] T. Regge and J. Wheeler, Phys. Rev. **108**, 1063 (1957).
[7] F. Zerilli, Phys. Rev. D **2**, 2141 (1970).
[8] K. Martel and E. Poisson, Phys. Rev. D **71**, 104003 (2005).
[9] S. Hopper and C. R. Evans, Phys. Rev. D **82**, 084010 (2010).
[10] S. Hopper and C. R. Evans, Phys. Rev. D **87**, 064008 (2013).
[11] S. Teukolsky, Astrophys. J. **185**, 635 (1973).
[12] P. L. Chrzanowski, Phys. Rev. D **11**, 2042 (1975).
[13] L. S. Kegeles and J. M. Cohen, Phys. Rev. D **19**, 1641 (1979).
[14] M. van de Meent, Phys. Rev. D **97**, 104033 (2018).
[15] A. Pound, Phys. Rev. Lett. **109**, 051101 (2012).
[16] A. Pound and J. Miller, Phys. Rev. D **89**, 104020 (2014).
[17] J. Miller, B. Wardell, and A. Pound, Phys. Rev. D **94**, 104018 (2016).
[18] A. Pound, Phys. Rev. D **95**, 104056 (2017).
[19] A. Pound, B. Wardell, N. Warburton, and J. Miller, Phys. Rev. Lett. **124**, 021101 (2020).
[20] L. Blanchet, Living Rev. Relativity **17**, 2 (2014).
[21] A. Buonanno and T. Damour, Phys. Rev. D **59**, 084006 (1999).
[22] T. Damour, Phys. Rev. D **64**, 124013 (2001).
[23] T. Damour, Phys. Rev. D **81**, 024017 (2010).
[24] B. P. Abbott *et al.* (The LIGO Scientific and VIRGO Collaborations), Phys. Rev. Lett. **116**, 061102 (2016).
[25] B. P. Abbott *et al.* (The LIGO Scientific and VIRGO Collaborations), Phys. Rev. Lett. **116**, 241103 (2016).
[26] B. P. Abbott *et al.* (The LIGO Scientific and VIRGO Collaborations), Phys. Rev. Lett. **116**, 221101 (2016).
[27] B. P. Abbott *et al.* (The LIGO Scientific and VIRGO Collaborations), Phys. Rev. X **6**, 041014 (2016).
[28] B. P. Abbott *et al.* (The LIGO Scientific and VIRGO Collaborations), Phys. Rev. Lett. **118**, 221101 (2017).
[29] B. P. Abbott *et al.* (The LIGO Scientific and VIRGO Collaborations), Phys. Rev. X **9**, 031040 (2019).
[30] B. P. Abbott *et al.* (The LIGO Scientific and VIRGO Collaborations), Phys. Rev. Lett. **119**, 161101 (2017).
[31] B. P. Abbott *et al.* (The LIGO Scientific and VIRGO Collaborations), Astrophys. J. Lett. **848**, L12 (2017).
[32] B. P. Abbott *et al.* (The LIGO Scientific and VIRGO Collaborations), Astrophys. J. Lett. **848**, L13 (2017).
[33] The LIGO Scientific and the Virgo Collaborations, arXiv:2004.08342.
[34] B. P. Abbott *et al.* (The LIGO Scientific and VIRGO Collaborations), Astrophys. J. Lett. **896**, L44 (2020).
[35] A. Bohé, L. Shao, A. Taracchini, A. Buonanno, S. Babak, I. W. Harry, I. Hinder, S. Ossokine, M. Pürrer, V. Raymond, T. Chu, H. Fong, P. Kumar, H. P. Pfeiffer, M. Boyle, D. A. Hemberger, L. E. Kidder, G. Lovelace, M. A. Scheel, and B. Szilágyi, Phys. Rev. D **95**, 044028 (2017).
[36] R. Cotesta, A. Buonanno, A. Bohé, I. Taracchini, A. Hinder, and S. Ossokine, Phys. Rev. D **98**, 084028 (2018).
[37] S. Ossokine, A. Buonanno, S. Marsat, R. Cotesta, S. Babak, T. Dietrich, R. Haas, I. Hinder, H. P. Pfeiffer, M. Pürrer, C. J. Woodford, M. Boyle, L. E. Kidder, M. A. Scheel, and B. Szilágyi, Phys. Rev. D **102**, 044055 (2020).
[38] S. Detweiler, Phys. Rev. D **77**, 124026 (2008).
[39] N. Sago, L. Barack, and S. L. Detweiler, Phys. Rev. D **78**, 124024 (2008).
[40] L. Barack and N. Sago, Phys. Rev. Lett. **102**, 191101 (2009).
[41] L. Blanchet, S. Detweiler, A. Le Tiec, and B. F. Whiting, Phys. Rev. D **81**, 064004 (2010).
[42] L. Blanchet, S. Detweiler, A. Le Tiec, and B. F. Whiting, Phys. Rev. D **81**, 084033 (2010).
[43] R. Fujita, Prog. Theor. Phys. **127**, 583 (2012).
[44] R. Fujita, Prog. Theor. Phys. **128**, 971 (2012).
[45] A. G. Shah, J. L. Friedman, and B. F. Whiting, Phys. Rev. D **89**, 064042 (2014).
[46] A. G. Shah, Phys. Rev. D **90**, 044025 (2014).
[47] S. R. Dolan, P. Nolan, A. C. Ottewill, N. Warburton, and B. Wardell, Phys. Rev. D **91**, 023009 (2015).
[48] N. K. Johnson-McDaniel, A. G. Shah, and B. F. Whiting, Phys. Rev. D **92**, 044007 (2015).
[49] D. Bini, T. Damour, and A. Geralico, Phys. Rev. D **93**, 064023 (2016).
[50] C. Kavanagh, A. C. Ottewill, and B. Wardell, Phys. Rev. D **92**, 084025 (2015).
[51] S. Akcay, A. Le Tiec, L. Barack, N. Sago, and N. Warburton, Phys. Rev. D **91**, 124014 (2015).
[52] N. Sago and R. Fujita, Prog. Theor. Exp. Phys. (**2015**), 073E03.
[53] E. Forseth, C. R. Evans, and S. Hopper, Phys. Rev. D **93**, 064058 (2016).
[54] S. Hopper, C. Kavanagh, and A. C. Ottewill, Phys. Rev. D **93**, 044010 (2016).
[55] C. Kavanagh, A. C. Ottewill, and B. Wardell, Phys. Rev. D **93**, 124038 (2016).
[56] D. Bini, T. Damour, and A. Geralico, Phys. Rev. D **93**, 064023 (2016).
[57] D. Bini, T. Damour, and A. Geralico, Phys. Rev. D **93**, 104017 (2016).
[58] D. Bini, T. Damour, and A. Geralico, Phys. Rev. D **93**, 124058 (2016).
[59] A. Nagar and A. Shah, Phys. Rev. D **94**, 104017 (2016).
[60] N. Sago, R. Fujita, and H. Nakano, Phys. Rev. D **93**, 104023 (2016).
[61] C. Kavanagh, D. Bini, T. Damour, S. Hopper, A. Ottewil, and B. Wardell, Phys. Rev. D **96**, 064012 (2017).
[62] D. Bini, T. Damour, A. Geralico, C. Kavanagh, and M. van de Meent, Phys. Rev. D **98**, 104062 (2018).
[63] D. Bini, T. Damour, A. Geralico, C. Kavanagh, and M. van de Meent, Phys. Rev. D **97**, 104022 (2018).
[64] D. Bini and A. Geralico, Phys. Rev. D **98**, 064026 (2018).
[65] D. Bini and A. Geralico, Phys. Rev. D **98**, 064040 (2018).
[66] D. Bini and A. Geralico, Phys. Rev. D **98**, 084021 (2018).
[67] D. Bini, T. Damour, and A. Geralico, Phys. Rev. D **97**, 104046 (2018).

[68] D. Bini and A. Geralico, Phys. Rev. D **100**, 104002 (2019).
[69] D. Bini and A. Geralico, Phys. Rev. D **100**, 104003 (2019).
[70] D. Bini and A. Geralico, Phys. Rev. D **100**, 121502 (2019).
[71] A. Nagar, F. Messina, C. Kavanagh, G. Lukes-Gerakopoulos, N. Warburton, S. Bernuzzi, and E. Harms, Phys. Rev. D **100**, 104056 (2019).
[72] C. Munna and C. R. Evans, Phys. Rev. D **100**, 104060 (2019).
[73] C. Munna and C. R. Evans, Phys. Rev. D **102**, 104006 (2020).
[74] A. Antonelli, C. Kavanagh, M. Khalil, J. Steinhoff, and J. Vines, Phys. Rev. Lett. **125**, 011103 (2020).
[75] D. Bini, T. Damour, and A. Geralico, arXiv:2003.11891.
[76] D. Bini, T. Damour, and A. Geralico, arXiv:2004.05407.
[77] S. Mano, H. Suzuki, and E. Takasugi, Prog. Theor. Phys. **96**, 549 (1996).
[78] D. Bini and T. Damour, Phys. Rev. D **87**, 121501 (2013).
[79] D. Bini and T. Damour, Phys. Rev. D **89**, 064063 (2014).
[80] D. Bini and T. Damour, Phys. Rev. D **90**, 024039 (2014).
[81] D. Bini and T. Damour, Phys. Rev. D **90**, 124037 (2014).
[82] R. Fujita, Prog. Theor. Exp. Phys. (**2015**), 033E01.
[83] T. Hinderer and E. E. Flanagan, Phys. Rev. D **78**, 064028 (2008).
[84] T. Osburn, N. Warburton, and C. R. Evans, Phys. Rev. D **93**, 064024 (2016).
[85] L. Barack and C. Cutler, Phys. Rev. D **75**, 042003 (2007).
[86] C. Hopman and T. Alexander, Astrophys. J. **629**, 362 (2005).
[87] C. Munna, C. R. Evans, S. Hopper, and E. Forseth, Phys. Rev. D **102**, 024047 (2020).
[88] H. R. P. Ferguson, D. H. Bailey, and S. Arno, J. Comb. Math. Comb. Comput. **68**, 351 (1999).
[89] S. Akcay, L. Barack, T. Damour, and N. Sago, Phys. Rev. D **86**, 104041 (2012).
[90] N. K. Johnson-McDaniel, Phys. Rev. D **90**, 024043 (2014).
[91] Black Hole Perturbation Toolkit," bhptoolkit.org.
[92] See Supplemental Material at http://link.aps.org/supplemental/10.1103/PhysRevD.102.124001 for the explicit high-order expansions in *Mathematica* format.
[93] T. Damour, P. Jaranowski, and G. Schäfer, Phys. Rev. D **89**, 064058 (2014).
[94] K. G. Arun, L. Blanchet, B. R. Iyer, and M. S. S. Qusailah, Phys. Rev. D **77**, 064034 (2008).
[95] K. G. Arun, L. Blanchet, B. R. Iyer, and M. S. S. Qusailah, Phys. Rev. D **77**, 064035 (2008).
[96] R.-M. Memmesheimer, A. Gopakumar, and G. Schäfer, Phys. Rev. D **70**, 104011 (2004).
[97] A. Le Tiec, L. Blanchet, and B. Whiting, Phys. Rev. D **85**, 064039 (2012).
[98] T. Damour, A. Nagar, and S. Bernuzzi, Phys. Rev. D **87**, 084035 (2013).
[99] C. Misner, K. Thorne, and J. Wheeler, *Gravitation* (Freeman, San Francisco, CA, U.S.A., 1973).
[100] M. Sasaki and H. Tagoshi, Living Rev. Relativity **6**, 6 (2003).
[101] S. Chandrasekhar, R. Soc. Proc. A **343**, 289 (1975).
[102] S. Chandrasekhar and S. Detweiler, R. Soc. Proc. A **345**, 145 (1975).
[103] S. Chandrasekhar, *The Mathematical Theory of Black Holes*, The International Series of Monographs on Physics Vol. 69 (Clarendon, Oxford, 1983).
[104] M. Berndston, Harmonic gauge perturbations of the Schwarzschild metric, Ph. D. thesis, University of Colorado, 2007, arXiv:0904.0033v1.
[105] L. Barack, A. Ori, and N. Sago, Phys. Rev. D **78**, 084021 (2008).
[106] E. E. Flanagan and T. Hinderer, Phys. Rev. Lett. **109**, 071102 (2012).
[107] S. Drasco, É. É. Flanagan, and S. A. Hughes, Classical Quantum Gravity **22**, S801 (2005).
[108] S. A. Hughes, S. Drasco, E. E. Flanagan, and J. Franklin, Phys. Rev. Lett. **94**, 221101 (2005).
[109] S. Drasco and S. A. Hughes, Phys. Rev. D **73**, 024027 (2006).
[110] R. Fujita, W. Hikida, and H. Tagoshi, Prog. Theor. Phys. **121**, 843 (2009).
[111] A. Taracchini, A. Buonanno, S. Hughes, and G. Khanna, Phys. Rev. D **88**, 044001 (2013).
[112] T. Tanaka, H. Tagoshi, and M. Sasaki, Prog. Theor. Phys. **96**, 1087 (1996).
[113] S. Isoyama, R. Fujita, N. Sago, H. Tagoshi, and T. Tanaka, Phys. Rev. D **87**, 024010 (2013).
[114] T. Damour and A. Nagar, Phys. Rev. D **76**, 064028 (2007).
[115] T. Damour, B. Iyer, and A. Nagar, Phys. Rev. D **79**, 064004 (2009).
[116] Y. Pan, A. Buonanno, R. Fujita, E. Racine, and H. Tagoshi, Phys. Rev. D **83**, 064003 (2011).
[117] F. Messina and A. Nagar, Phys. Rev. D **95**, 124001 (2017).
[118] F. Messina, A. Maldarella, and A. Nagar, Phys. Rev. D **97**, 084016 (2018).
[119] A. Nagar, G. Pratten, G. Riemenschneider, and R. Gamba, Phys. Rev. D **101**, 024041 (2020).
[120] D. Chiaramello and A. Nagar, Phys. Rev. D **101**, 101501 (2020).
[121] R. Fujita, N. Sago, and H. Nakano, Classical Quantum Gravity **35**, 027001 (2018).
[122] S. Akcay, S. Dolan, C. Kavanagh, J. Moxon, N. Warburton, and B. Wardell, arXiv:1912.09461.
[123] M. Casals and A. C. Ottewill, Phys. Rev. D **92**, 124055 (2015).
[124] C. Darwin, Proc. R. Soc. A **249**, 180 (1959).
[125] C. Cutler, D. Kennefick, and E. Poisson, Phys. Rev. D **50**, 3816 (1994).
[126] L. Barack and N. Sago, Phys. Rev. D **81**, 084021 (2010).
[127] I. S. Gradshteyn, I. M. Ryzhik, A. Jeffrey, and D. Zwillinger, *Table of Integrals, Series, and Products*, 7th ed. (Elsevier Academic Press, New York, 2007), ISBN .
[128] C. Munna and C. R. Evans, Phys. Rev. D (to be published).
[129] P. C. Peters and J. Mathews, Phys. Rev. **131**, 435 (1963).
[130] R. V. Wagoner and C. M. Will, Astrophys. J. **210**, 764 (1976).
[131] K. G. Arun, L. Blanchet, B. R. Iyer, and S. Sinha, Phys. Rev. D **80**, 124018 (2009).
[132] P. C. Peters, Phys. Rev. **136**, B1224 (1964).
[133] L. Blanchet and G. Schäfer, Classical Quantum Gravity **10**, 2699 (1993).
[134] L. Blanchet, T. Damour, and B. R. Iyer, Phys. Rev. D **51**, 5360 (1995).
[135] L. Blanchet, Phys. Rev. D **54**, 1417 (1996).

[136] E. R. Forseth, High-precision extreme-mass-ratio inspirals in black hole perturbation theory and post-Newtonian theory, Ph.D. Thesis, The University of North Carolina at Chapel Hill, 2016.
[137] W. Goldberger and A. Ross, Phys. Rev. D **81**, 124015 (2010).
[138] S. Isoyama, R. Fujita, H. Nakano, N. Sago, and T. Tanaka, Prog. Theor. Exp. Phys. (**2013**), 063E01.
[139] T. Damour and N. Deruelle, Ann. Inst. Henri Poincaré Phys. Théor. **43**, 107 (1985).
[140] T. Damour and G. Schäfer, Nuovo Cimento B **101B**, 127 (1988).
[141] G. Schäfer and N. Wex, Phys. Lett. **174**, 196 (1993).
[142] P. Fromholtz, E. Poisson, and C. Will, Am. J. Phys. **82**, 295 (2014).
[143] L. Barack, T. Damour, and N. Sago, Phys. Rev. D **82**, 084036 (2010).
[144] D. Bini, T. Damour, and A. Geralico, Phys. Rev. Lett. **123**, 231104 (2019).
[145] C. Munna and C. R. Evans, Phys. Rev. D (to be published).
[146] S. Deser, Gen. Relativ. Gravit. **46**, 1615 (2014).
[147] L. Barack and N. Sago, Phys. Rev. D **83**, 084023 (2011).
[148] A. Pound, C. Merlin, and L. Barack, arXiv:1310.1513.
[149] J. Thompson, B. Wardell, and B. Whiting, Phys. Rev. D **99**, 124046 (2019).